

## Two different types of granitoids in the Suyunhe large porphyry Mo deposit, NW China and their genetic relationships with molybdenum mineralization



Shihua Zhong <sup>a,b</sup>, Reimar Seltmann <sup>c,\*</sup>, Ping Shen <sup>b</sup>

<sup>a</sup> MLR Key Laboratory of Metallogeny and Mineral Assessment, Institute of Mineral Resources, Chinese Academy of Geological Sciences, Beijing 100037, China

<sup>b</sup> Key Laboratory of Mineral Resources, Institute of Geology and Geophysics, Chinese Academy of Sciences, Beijing 100029, China

<sup>c</sup> Center for Russian and Central EurAsian Mineral Studies, Department of Earth Sciences, Natural History Museum, London SW7 5BD, UK

### ARTICLE INFO

#### Article history:

Received 31 December 2016

Received in revised form 16 April 2017

Accepted 19 April 2017

Available online 21 April 2017

#### Keywords:

Porphyry Mo deposit

Adakite

Ce<sup>4+</sup>/Ce<sup>3+</sup>

Suyunhe

West Junggar

### ABSTRACT

The Suyunhe large porphyry Mo deposit (~0.57 Mt molybdenum), located in the West Junggar, NW China, is the largest known porphyry Mo deposit in Xinjiang. Granitoids in this deposit are mainly characterized by three closely spaced intrusive centers (known as stocks I, II and III respectively). The stocks I and III mainly consist of barren granodiorite porphyry and tonalite porphyry, whereas the stock II is mainly composed of fertile monzonitic granite porphyry and granite porphyry. Based on detailed major and trace element, and Sr–Nd isotopic analyses, two distinct compositional groups can be identified. The first group of high-silica end-members (HSE) is characterized by high SiO<sub>2</sub> (mostly >75 wt%), low MgO (0.07–0.69 wt%) and Mg# (0.19–0.36), significant Eu depletion in the chondrite-normalized diagram, and low Sr/Y and La/Yb, as well as noticeably negative anomalies of Ba, Sr, P and Ti in the primitive mantle-normalized diagram. The second group of low-silica end-members (LSE), however, displays adakite-like features with lower SiO<sub>2</sub> (<75 wt%), higher MgO (0.52–1.32 wt%) and Mg# (0.32–0.52; mostly >0.4), and higher Sr/Y (mostly >20) and La/Yb (>8). The depleted Sr–Nd isotopic characteristics ( $\varepsilon_{\text{Nd}}(T) = 3.5\text{--}6.4$  and  $I_{\text{Sr}} = 0.7026\text{--}0.7055$ ) and young two-stage model ages of HSE and LSE indicate that they were both derived from partial melting of juvenile lower crust that might be triggered by asthenosphere upwelling subsequent to a slab rollback event. However, the depths of initial melting might be different. The current evidence demonstrates that HSE in the Suyunhe deposit formed by partial melting of juvenile crust at depths of less than ~33 km with a plagioclase residue, whereas that for LSE occurred at depths of >40 km where a garnet residue existed and the crust was thickened. The lower source depth, as well as subsequently strong plagioclase fractionation, results in the absence of adakite-like characteristics in HSE.

The Ce<sup>4+</sup>/Ce<sup>3+</sup> and Eu<sub>N</sub>/Eu<sub>N\*</sub> ratios in zircons of HSE are much lower than ore-forming intrusions from porphyry Cu deposits in the Central Asian Orogenic Belt, but noticeably higher than barren intrusions from the Lachlan fold belt and ore-bearing intrusions from small-intermediate porphyry Mo deposits from the East Qinling–Dabie and the Nanling metallogenic belts, China, indicating that neither too high nor too low oxygen fugacities are favorable for large porphyry Mo deposits. Based on previous studies of adakitic rocks in the world, adakite-like LSE in the Suyunhe deposit are believed to have higher oxygen fugacities, and thus be less fertile than HSE. We finally suggest that adakites and adakite-like rocks are unproductive for porphyry Mo deposits.

© 2017 Elsevier B.V. All rights reserved.

### 1. Introduction

The Central Asian Orogenic Belt (CAOB; Fig. 1a), formed by complicated subduction–accretion processes of the Palaeo-Asian Ocean

from the late Mesoproterozoic to Mesozoic (c. 1000–250 Ma), is a large accretionary orogenic collage in a manner comparable with that of circum-pacific Mesozoic–Cenozoic orogens (Windley et al., 2007; Xiao et al., 2009c; Xu et al., 2013; Xiao and Santosh, 2014). It is not only famous for the unique conditions to study continental growth (Prajno et al., 2008; Xiao et al., 2009a; Tang et al., 2010, 2012a; Safonova et al., 2011; Seltmann et al., 2011; Yin et al.,

\* Corresponding author.

E-mail address: [r.seltmann@nhm.ac.uk](mailto:r.seltmann@nhm.ac.uk) (R. Seltmann).

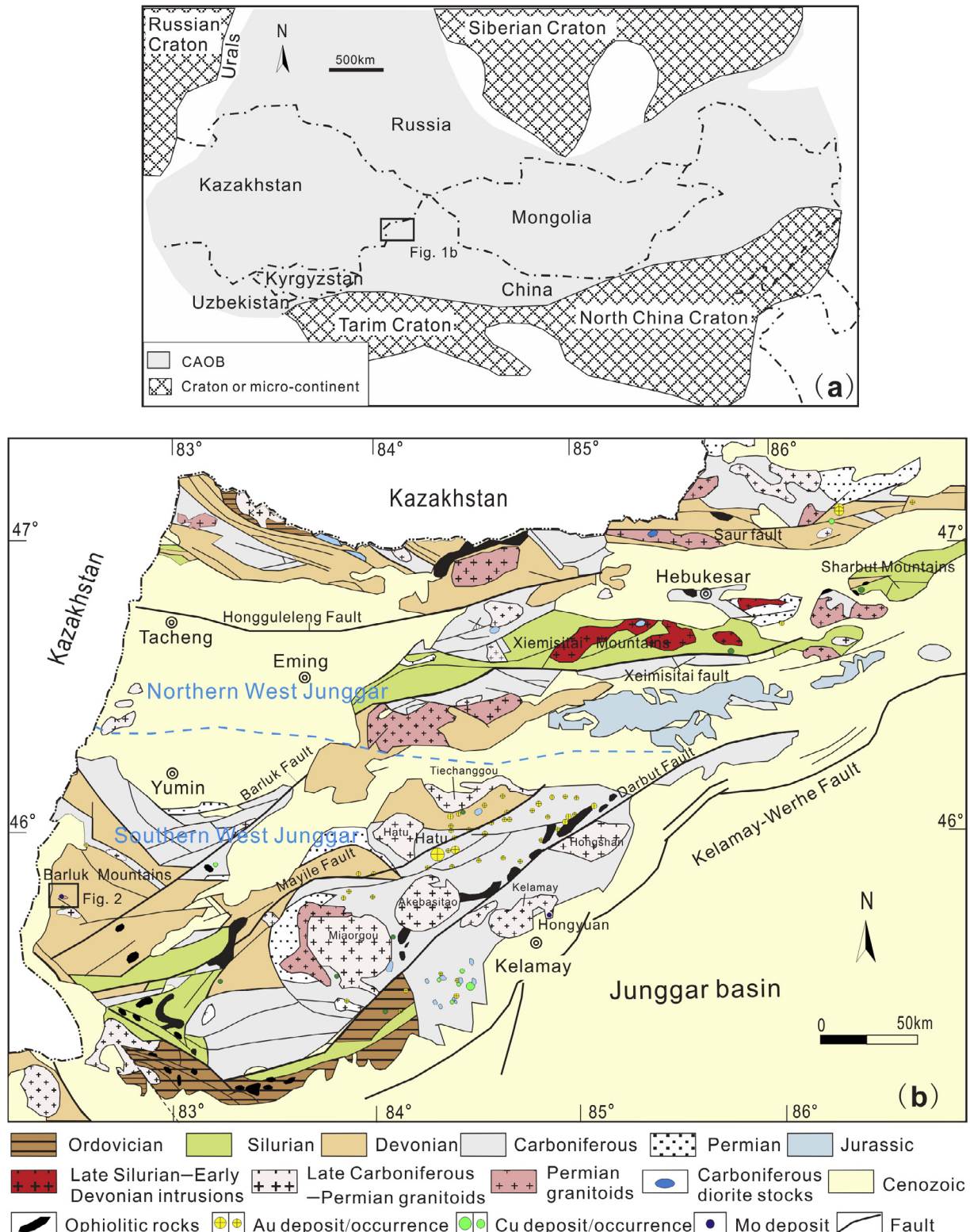


**Fig. 1.** (a) Schematic map of the Central Asian Orogenic Belt (modified after Shen et al., 2013b; Xiao et al., 2009b). The rectangle represents the West Junggar region. (b) Geological map of the West Junggar region (modified after Shen et al., 2013b). The square represents the Suyunhe large porphyry Mo deposit.

2013, 2015a–c; Kröner et al., 2014), but also for the occurrence of the giant porphyry Cu–Mo–Au deposits (Pirajno et al., 2011; Dolgopolova et al., 2013; Shen et al., 2015). The West Junggar terrain, located between the Yili terrane to the south and the Palaeozoic Chinese Altai magmatic arc to the north (Fig. 1b) (Pirajno

et al., 2011; Xu et al., 2013), is an important part of the CAOB. Over the last decade, numerous studies in this area have focused on Late Carboniferous–Early Permian intrusions because of their significance in understanding the evolution histories of the CAOB (Tang et al., 2010, 2012a,b; Yin et al., 2013, 2015a). Recently, a

few porphyry Cu–Mo deposits were discovered in the West Junggar (Shen et al., 2013b, 2017; Shen and Pan, 2013, 2015; Cao et al., 2014, 2016; Li et al., 2014, 2016; Zhong et al., 2015a) and most of them were found to be related to Late Carboniferous–Early Permian intrusions. However, the origin and evolution processes of ore-forming magmas are still poorly studied. Moreover, few studies have been designed exclusively to reveal the relationships between Mo mineralization and those intrusions in the West Junggar.

The Suyunhe porphyry Mo deposit, discovered by No.1 Regional Geological Survey Party of Xinjiang Bureau of Geology and Mineral Exploration and Development, Urumchi (NO.1 RGSPXBGMEDU), is located in the SW 96 km of Yumin country, Xinjiang ( $45^{\circ}47'15''$  N,  $82^{\circ}28'30''$  E; Fig. 1b). Currently, it is the largest porphyry Mo deposit in the West Junggar with a metal resource of  $\sim 0.57$  Mt. Three stocks, referred to as stocks I, II and III respectively, developed in this deposit, and were believed to be related to Mo mineralization. Geochronological and geochemical work on these stocks were conducted by Zhong et al. (2015a) and Shen et al. (2017), arguing that they formed in Late Carboniferous to Early Permian and were mainly highly fractionated I-type granites, although the exact intrusion age is controversial. However, Yang et al. (2015) found that some granites in the Suyunhe deposit exhibited adakitic signatures (Fig. 9 in their article). A detailed work has not been conducted to illustrate their genesis. Besides, some granitoids in the Suyunhe deposit (e.g., tonalite porphyry) are barren, whereas others (e.g., monzonitic granite porphyry and granite porphyry) are fertile. The reasons resulting in the discrepancies of productivity among these granitoids are unclear and our research aims to resolve this dilemma.

In this paper, new major and trace elemental and Sr–Nd isotopic data of whole-rock, as well as trace element data of zircon, are presented. Combined with previously published data, the high-quality geochemical database gives convincingly tight constraints on the origin of the Suyunhe granitoids, as well as on the relationship of the magmatic oxidation state and mineralization. Furthermore, this study also puts advanced and new insights into the role of magmas in controlling the types and origin of mineralization in the CAOB.

## 2. Geological setting

### 2.1. Geology of the southern West Junggar

The West Junggar fold belt mainly consists of Palaeozoic volcanic arc in the northern part and accretionary complexes in the southern part that were accreted onto the Kazakhstan plate as the Tarim, Kazakhstan, and Siberian plates converged (Shen et al., 2013a). The Suyunhe Mo deposit is located in the southern West Junggar (Fig. 1b).

Precambrian basement rocks have not been discovered in this area (Chen and Arakawa, 2005; Tang et al., 2010, 2012b; Yin et al., 2010). Many Paleozoic ophiolitic mélange, however, have been documented with ages mainly ranging from Cambrian to Early Carboniferous (Zhang and Huang, 1992; Yang et al., 2012a, 2013; Zhao et al., 2013; Wen et al., 2016; Weng et al., 2016). Recently, Yang et al. (2012b) reported the age of the Mayile ophiolite ( $572 \pm 9$  Ma; Neoproterozoic) and argued that it was the oldest ophiolite found in this area. The accepted youngest ophiolite in the West Junggar is the Darbut ophiolite, although its age is controversial from  $395 \pm 12$  Ma to  $302 \pm 2$  Ma (Zhang and Huang, 1992; Xu et al., 2006; Liu et al., 2009; Yang et al., 2012a). The strata in this area are characterized by the occurrence of Devonian–Carboniferous volcano-sedimentary strata, with the Devonian strata mainly located in the west of Mayile fault and the Carboniferous strata mainly located in areas of the Darbut fault (Fig. 1b). These strata

were intruded by large numbers of Late Carboniferous–Early Permian plutons (Fig. 1b). Late Carboniferous deep water sedimentary rocks were reported in the West Junggar, suggesting a Late Carboniferous deep-marine environment (Jin et al., 1987; Song et al., 1996). Volcanic rocks and dikes are also abundant in this area (Li et al., 2004; Tang et al., 2010). The former (i.e. volcanic rocks) consists of andesitic basalt, andesite, felsic tuff and minor quartz or olivine tholeiite (Shen and Jin, 1993; Yin et al., 2013), and recently published geochronological and geochemical data with regard to these volcanic rocks indicate a subduction-related setting at 350–296 Ma (Wang and Zhu, 2007; Geng et al., 2011; Tang et al., 2012c); the latter is mainly intermediate–basaltic in compositions and normally cuts granitoid intrusions and carboniferous strata (Li et al., 2004; Yin et al., 2010).

The Late Carboniferous–Early Permian plutons in the southern West Junggar are composed of huge batholiths and small intermediate–felsic stocks. Huge batholiths, such as Tiechanggou, Hatu, Akebasitao, Miaoergou, Hongshan and Kelamayi batholiths, were located in the areas of the Darbut fault and emplaced at 316–300 Ma (Chen and Arakawa, 2005; Geng et al., 2009; Tang et al., 2012a,b) (Fig. 1b). They are recently argued to be related to oceanic ridge subduction in Late Carboniferous in the West Junggar (Geng et al., 2009). Small intermediate–felsic stocks, mainly located in the regions of the Darbut and Barluk faults, such as Bieluagaxi (Yin et al., 2015a), Baogutu, Hongyuan, Shiwu and Suyunhe intrusions, are mainly dioritic, granodioritic and monzonitic in compositions and closely related to porphyry Cu–Mo mineralization in this region (Li et al., 2016; Shen et al., 2010, 2013b, 2017; Yan et al., 2014; Zhong et al., 2015a). Noticeably, existence of adakites is firmly confirmed in the Baogutu area of the West Junggar (Geng et al., 2009; Tang et al., 2012a,b). These adakites are considered to be derived from partial melting of subducted oceanic crust that was induced by slab window-related upwelling asthenosphere (Tang et al., 2010, 2012a; Tang et al., 2012c; Yin et al., 2013).

### 2.2. Geology of the Suyunhe porphyry Mo deposit

The Suyunhe large porphyry Mo deposit is located in the southwest of the West Junggar (Fig. 1b). Detailed descriptions about strata, mineralization, alteration and intrusive histories were given by Zhong et al. (2015a, 2015b) and Shen et al. (2017) that we summarize here.

The Middle Devonian Barluk Group is the only outcropped strata in the Suyunhe deposit (Fig. 2), and is composed of crystal-vitrific tuff, tuffaceous siltstone, sedimentary tuff and pebbly grey-wacke. The structural pattern is dominantly characterized by the NE-trending fault, whereas ENE-, and NW-trending faults are also present (Fig. 2). The distribution of mineralization in the Suyunhe deposit is mainly controlled by three closely spaced intrusive centers referred to as stocks I, II and III respectively (Fig. 2). Both felsic stocks and their wall rocks host Mo mineralization, although differences can be seen in three stocks. The Mo mineralization related to stocks I and III is mainly distributed in the strata with Mo ore resources of 19.4 Mt and 1.4 Mt respectively, whereas that related to stock II is mainly distributed in the intrusions with Mo ore resources of 35.3 Mt. These stocks are cut by a number of felsic and intermediate dikes (Fig. 2). The orebodies have lenticular forms and have no distinct boundaries with country rocks, showing gradational contact relationships. Mineralization in the Suyunhe is dominantly stockworks with minor dissemination. Main ore minerals include molybdenite, scheelite, pyrite, and chalcopyrite, with minor chalcocite, bornite, ilmenite, and pyrrhotite; Gangue minerals are dominated by quartz, K-feldspar, plagioclase, and biotite. Although alteration associated with Mo mineralization (e.g., potassic, chlorite–muscovite, and phyllitic alteration) can be seen,

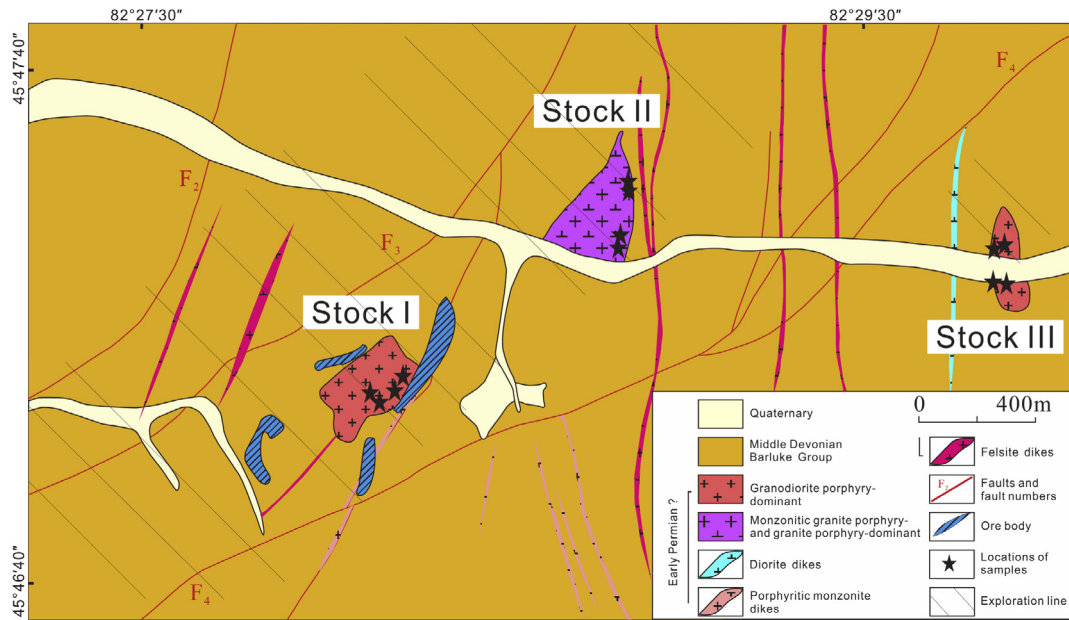


**Fig. 2.** Geological map of the Suyunhe large porphyry Mo deposit. Based on Zhong et al. (2015a) and Shen et al. (2017).

a well-developed alteration zoning, commonly seen in typical porphyry deposits, is not manifested currently in the Suyunhe deposit.

Petrographic observations show that all the stocks are composed of deep granites and shallower porphyries. The shallow porphyries in stock I mainly consist of granodiorite porphyry, monzonitic granite porphyry and tonalite porphyry, those in stock II are mainly composed of granite porphyry and monzonitic granite porphyry, whereas those in stock III consist mainly of granodiorite porphyry, tonalite porphyry and minor granite porphyry (Fig. 2). Due to unfavourable outcrop situation in the Suyunhe deposit, the exact emplaced sequence of the porphyries is still unclear. Although granite, granodiorite porphyry, granite porphyry, and monzonitic granite porphyry are all ore-bearing, the latter two are the most enriched hosts to mineralization. The tonalite porphyry, however, is nearly barren.

### 3. Petrography

Mineralogically, monzonitic granite porphyry contains phenocrysts of plagioclase (25–30 vol%, An<sub>15–48</sub>) and K-feldspar (30–35 vol%), minor biotite (5–10 vol%) in a groundmass of plagioclase, quartz and K-feldspar. The granite porphyry contains phenocrysts of more K-feldspar (ca. 40 vol%), less plagioclase (ca. 20 vol%) and quartz (5 vol%), and more biotite (15 vol%) in a groundmass of quartz, plagioclase and K-feldspar. The granodiorite porphyry contains phenocrysts of plagioclase (ca. 40 vol%) and minor K-feldspar (10–15 vol%), biotite (5–10 vol%), hornblende (ca. 5%), and quartz (5–10 vol%) in a groundmass of quartz, plagioclase and minor K-feldspar. The tonalite porphyry contains phenocrysts of plagioclase (30–40 vol%) and minor hornblende (5–10 vol%) and biotite (5–10 vol%) in a groundmass of plagioclase, quartz and minor K-feldspar. Accessory minerals in these granitoids are similar and include zircon, apatite, titanite, pyrite and magnetite. In general, mineral components of different types of granitoids in the Suyunhe are broadly similar and gradually varied, and therefore sometimes the identification is hard.

All the granitoids outcropping in the Suyunhe deposit were analyzed in this study and the least altered samples for geochemical

analysis were selected, therefore ensuring the accuracy and representativeness of the geological survey.

## 4. Analytical methods

### 4.1. Major and trace element contents of whole rocks

Nine samples were collected for major and trace element analyses and measured at the Institute of Geology and Geophysics, Chinese Academy of Sciences, Beijing. They were trimmed to remove weathered surfaces, cleaned with deionized water, crushed and then powdered with an agate mill.

Major oxides were analyzed with a XRF-1500 Sequential X-ray Fluorescence Spectrometry (XRF) on fused glass beads, with FeO and loss-on-ignition analyzed by wet chemical methods. Analytical uncertainties were better than 0.5% for all major elements. Trace elements were analyzed with a plasma optical emission mass spectrometer ICP-MS system. Detailed analytical procedures were given by Shen et al. (2012). The measurement error and drift were controlled by regular analyses of standard samples with a periodicity of 10%. Analyzed uncertainties of ICP-MS data at the ppm level were better than 10%.

### 4.2. Zircon trace elements analyses

Zircon trace elements analyses were carried out by employing an ArF excimer laser ablation system, attached to a Neptune Plasma multi-collector ICP-MS with a Geolas-193 laser-ablation system (LA-MC-ICP-MS), at the Institute of Geology and Geophysics, Chinese Academy of Sciences, Beijing. These zircons were selected from three samples (sample ZK0809-255 from stock I; sample ZK6019-507 from stock II; sample ZK9235-447 from stock III; see Appendix Table 1 for more details) and dated by Zhong et al. (2015a) using LA-ICP-MS. The zircon trace elements analyses were simultaneously carried out with U-Th-Pb analyses, with ablation pit of 60 µm in diameter, ablation time of 26 s and a laser pulse frequency of 6–8 Hz. The detailed analytical procedures were similar to those described by Yuan et al. (2004). Helium was used as a carrier gas to transport the ablated sample from the laser-ablation cell

to the ICP-MS torch via a mixing chamber where it was mixed with argon. NIST SRM 610 was used as a reference material and  $^{29}\text{Si}$  was used as the internal calibrant.

#### 4.3. Sr-Nd isotope compositions of whole rocks

Ten representative samples from the Suyunhe intrusions were selected for analyses of Rb, Sr, Sm and Nd isotope compositions, using a MAT-262 at Institute of Geology and Geophysics, Chinese Academy of Sciences, Beijing. Approximately 100–150 mg of whole rock powder was decomposed in a mixture of HF-HClO<sub>4</sub> in screw-top Teflon beakers, and Rb, Sr, Sm and Nd were separated by cation exchange columns, following the procedure of Chen et al. (2002). Procedural blanks were <100 pg for Sm and Nd, and <50 pg for Rb and Sr. The  $^{87}\text{Sr}/^{86}\text{Sr}$  ratios were normalized to  $^{86}\text{Sr}/^{88}\text{Sr} = 0.1194$  and the  $^{143}\text{Nd}/^{144}\text{Nd}$  ratios to  $^{146}\text{Nd}/^{144}\text{Nd} = 0.7219$ . The reported  $^{87}\text{Sr}/^{86}\text{Sr}$  and  $^{143}\text{Nd}/^{144}\text{Nd}$  ratios were adjusted to the NBS SRM 987 standard  $^{87}\text{Sr}/^{86}\text{Sr} = 0.71025$  and  $^{143}\text{Nd}/^{144}\text{Nd} = 0.512115$  respectively.

## 5. Results

### 5.1. Whole rock major and trace elements

The results of whole rock major and trace elements are shown in Table 1 and Supplementary Table 1. Using 9 major and trace element analyses from this article and 50 analyses published by Shen et al. (2013a, 2017), Yang et al. (2015) and Zhong et al. (2015a), two main compositional groups based on their silica contents are clearly shown and could be defined as low-silica end-members (LSE: SiO<sub>2</sub> <75 wt%) and high-silica end-members (HSE: mostly SiO<sub>2</sub> >75 wt%). Low-silica end-members include 12 rocks from stock I, and 11 rocks from stock III, whereas no sample from stock II could be encompassed by the low-silica subgroup. High-silica end-members include 16 rocks from stock I, all 13 samples from stock II, and 7 samples from stock III.

Mineralogically, LSE differ from HSE primarily in that they may contain amphibole phenocrysts. Apart from a lower silica content, LSE also have higher MgO (0.52–1.32 wt%) and Mg# (0.32–0.52;

**Table 1**  
Major (%) and trace element (ppm) analyses of granitoids in the Suyunhe large porphyry Mo deposit.

Sample No.	s1m2-1	s1m2-2	zk0805-200	zk6019-490	zk6019-492	zk6019-507	s3p2-4	s3p3-1	zk9235-462
Stock	I	I	I	II	II	II	III	III	III
Rock	MGP	MGP	MGP	GP	GP	GP	G	G	G
SiO <sub>2</sub>	74.86	73.95	73.92	75.85	74.52	75.47	70.93	72.4	75.62
Al <sub>2</sub> O <sub>3</sub>	13.11	13.1	13.12	12.34	12.95	12.81	14.24	14.01	12.52
TFeO	1.55	1.65	1.65	1.45	1.63	1.49	2.69	2.28	1.58
MgO	0.41	0.38	0.37	0.3	0.42	0.37	0.83	0.82	0.4
CaO	1.28	1.2	1.13	0.6	1	1.05	1.92	1.65	1.11
Na <sub>2</sub> O	3.76	3.67	4.04	3	3.86	3.74	3.73	4.3	3.51
K <sub>2</sub> O	4.04	4.52	4.01	5.58	4.14	4.2	3.49	2.78	4.19
MnO	0.05	0.05	0.05	0.04	0.06	0.05	0.06	0.1	0.06
TiO <sub>2</sub>	0.18	0.17	0.18	0.14	0.19	0.17	0.32	0.27	0.18
P <sub>2</sub> O <sub>5</sub>	0.05	0.05	0.05	0.04	0.05	0.04	0.11	0.09	0.04
LOI	0.68	1.19	0.78	0.4	0.64	0.3	1.56	1.26	0.26
Total	99.97	99.93	99.3	99.74	99.46	99.69	99.88	99.96	99.47
Ni	5.8	7.9	4.6	4.1	5.5	5.3	6.8	8.6	6.1
Ga	14.7	14.5	15.9	12.8	14.6	15.8	16.1	16.4	14.8
Rb	141	159	156.5	198	152.5	159	100	63.8	153
Sr	136	131	111.5	120.5	126	114	244	481	122
Ba	237	298	239	327	204	181	732	565	232
La	13.9	20.8	14.3	11.7	19.8	19.7	17.3	21	21.3
Ce	27.4	37.9	30.3	23.7	41.2	41.9	32.2	37.8	42.8
Pr	3.2	4.2	3.4	2.5	4.5	4.7	3.8	4.3	4.6
Nd	11.9	14.6	12.4	9.4	15.9	16.4	15.3	16.4	15.6
Sm	2.4	2.4	3.2	1.9	3.1	4	3.2	3.1	3.1
Eu	0.34	0.4	0.46	0.39	0.33	0.3	0.71	0.76	0.42
Gd	2.26	2.13	2.73	1.91	2.67	3.57	2.87	2.45	2.7
Tb	0.4	0.4	0.5	0.3	0.4	0.6	0.6	0.4	0.5
Dy	2.5	1.9	3.2	1.9	2.9	4.1	3.1	2.3	2.9
Ho	0.5	0.4	0.7	0.4	0.6	0.9	0.6	0.4	0.6
Er	1.9	1.4	2.4	1.4	1.8	2.9	1.9	1.4	2
Tm	0.4	0.3	0.4	0.2	0.3	0.5	0.3	0.2	0.3
Yb	2.5	2	3.4	1.7	2.7	3.9	2.1	1.6	2.6
Lu	0.4	0.3	0.6	0.3	0.4	0.7	0.3	0.2	0.4
Y	18.3	13.8	25.3	13.4	19.9	30.7	17.3	12.9	20.4
Pb	17.8	19	18.1	26.1	20.2	20.9	28.3	10.9	19.9
Th	15.4	13.4	17.1	14.1	16.1	17.5	7.8	6.3	16.3
U	6.3	4.9	9.8	6.2	7.6	10.3	3.4	2.7	6.8
Nb	10.6	9.3	15.8	7.4	13.2	13.4	7.4	6.7	9.5
Ta	1.2	0.8	1.9	0.9	1.3	2.3	0.8	0.5	1.1
Zr	97.3	89.5	123	59	99	91	146	135	87
Hf	3.7	3.3	4.7	2.8	3.8	4.2	4.5	3.9	3.4
A/CNK	1.02	1.00	1.01	1.02	1.02	1.02	1.06	1.07	1.02
Mg#	0.34	0.31	0.31	0.29	0.34	0.33	0.38	0.42	0.33
La/Yb	5.6	10.4	4.2	6.9	7.3	5.1	8.2	13.1	8.2
Sr/Y	7.4	9.5	4.4	9.0	6.3	3.7	14.1	37.3	6.0
Rb/Sr	1.0	1.2	1.4	1.6	1.2	1.4	0.4	0.1	1.3
$\delta\text{Eu}$	0.45	0.54	0.48	0.63	0.35	0.24	0.72	0.84	0.44

A = Al<sub>2</sub>O<sub>3</sub>, N = Na<sub>2</sub>O, K = K<sub>2</sub>O, C = CaO, Mg<sup>#</sup> = 100 \* Mg/(Mg+total Fe) (all in molar proportion).

Abbreviations: MGP, monzonitic granite porphyry; GP, granite porphyry; G, granite

mostly >0.4) compared to HSE ( $\text{MgO} = 0.07\text{--}0.69\text{ wt\%}$ ;  $\text{Mg}\# = 0.19\text{--}0.36$ ) (Fig. 3). Fig. 4 is chondrite-normalized rare earth elements (REE) and primitive mantle-normalized multi-element diagrams which show comparisons between LSE and HSE. It shows that (1) Eu negative anomalies are indistinctive in LSE whereas extremely noticeable in HSE (Fig. 4a and c); (2) although in both cases concave REE patterns are shown, LSE exhibit lower heavy rare

earth elements (HREE) than HSE (Fig. 4a and c); (3) compared to LSE, HSE show stronger enrichment in Th and U and more characteristic depletion in Ba, Sr, P and Ti (Fig. 4b and d). On the plot of  $\text{SiO}_2$  versus  $\delta\text{Eu}$  (Fig. 5),  $\delta\text{Eu}$  values of LSE are high (0.63–0.97) and roughly constant, whereas those of HSE are lower (mostly  $\delta\text{Eu} = 0.13\text{--}0.55$ ) and dramatically decrease with increasing  $\text{SiO}_2$ . Other significant differences can be seen in the major and trace

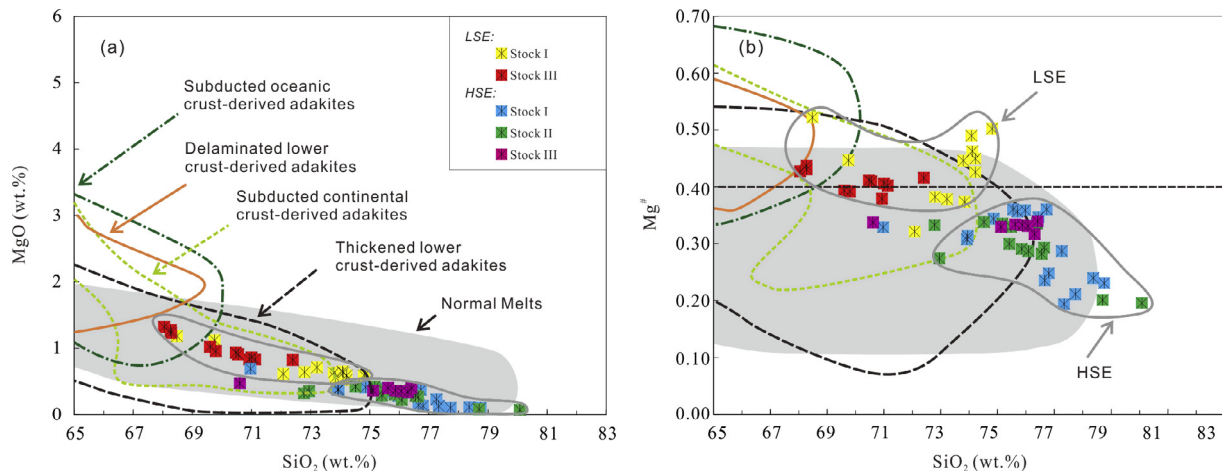


**Fig. 3.**  $\text{SiO}_2$  versus  $\text{MgO}$  (a) and  $\text{Mg}\#$  (b) diagrams. Fields for subducted oceanic and continental crust-derived adakites, thickened and delaminated mafic lower crust-derived adakites, and normal melts (i.e., metabasaltic and eclogite experimental melts; 1–4.0 GPa) are after Tang et al. (2010) and references therein.

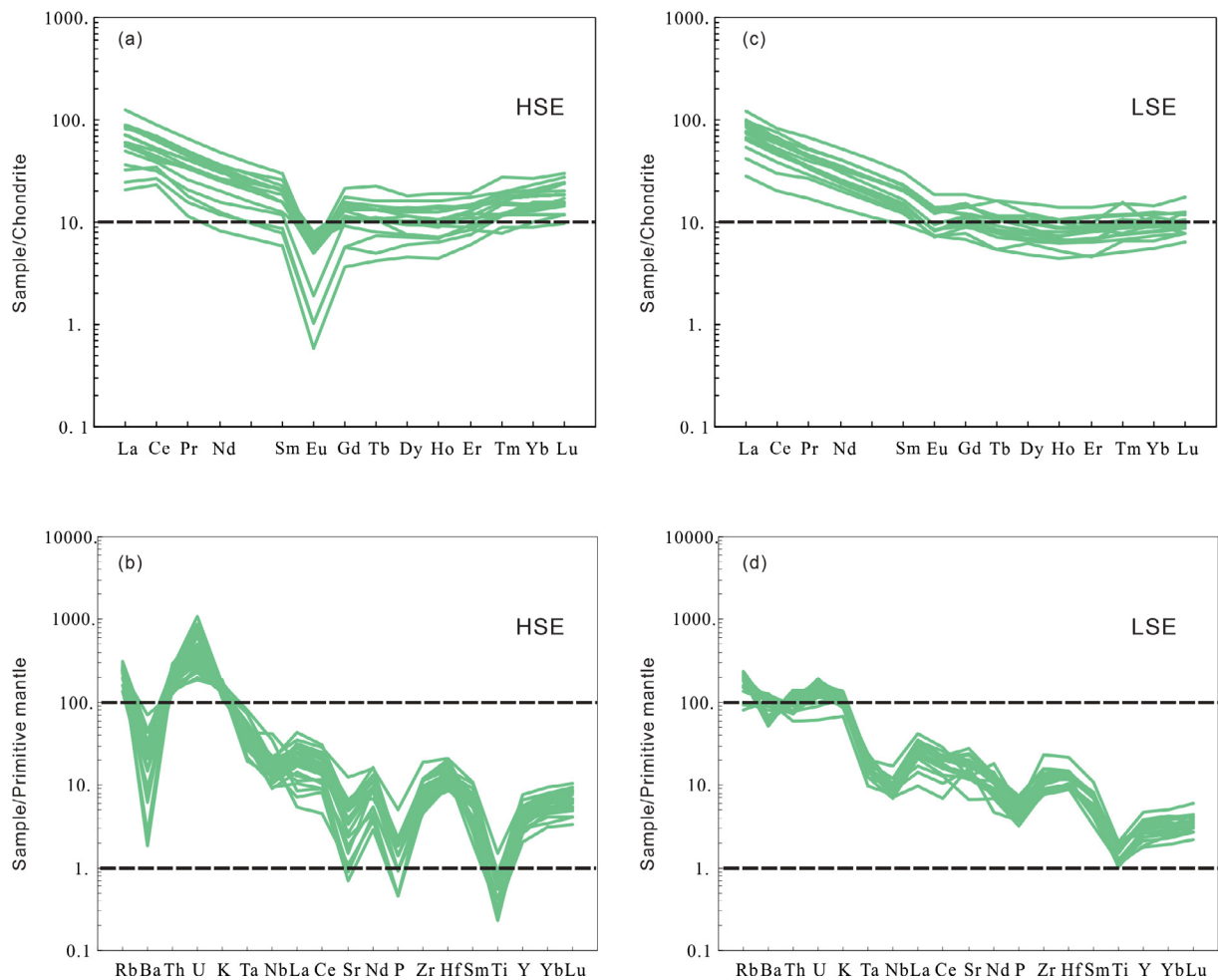


**Fig. 4.** Chondrite-normalized REE diagrams of the granitoids in the Suyunhe large porphyry Mo deposit. The normalization values are from Sun and McDonough (1989).

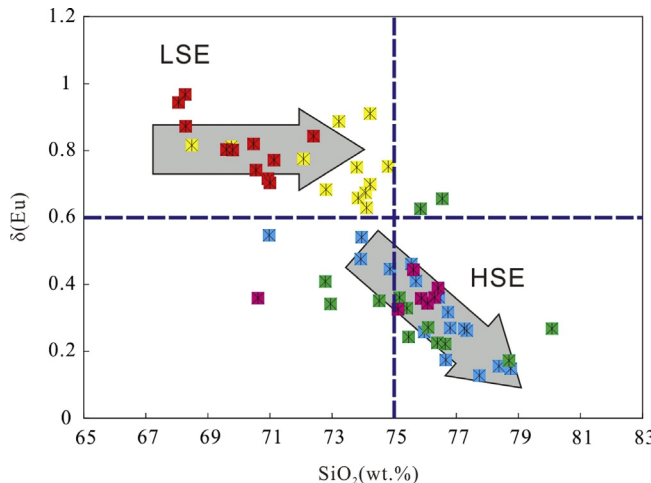


Fig. 5.  $\text{SiO}_2$  versus  $\delta(\text{Eu})$  diagram. Symbols are as in Fig. 3.

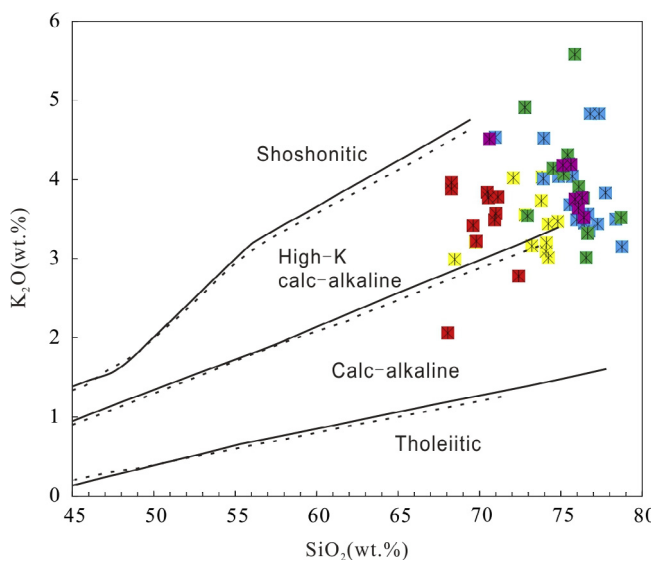


Fig. 6.  $\text{SiO}_2$  versus  $\text{K}_2\text{O}$  diagram. Symbols are as in Fig. 3.

element Harker diagrams as well as Y vs.  $\text{Sr}/\text{Y}$  and  $\text{Yb}$  vs.  $\text{La}/\text{Yb}$  plots; they are discussed below.

In spite of the pronounced distinctions, the two groups are both relatively high in  $\text{K}_2\text{O}$  contents (2.06 to 5.58 wt%) with variable ranges of  $\text{Na}_2\text{O}$  contents (0.17 to 4.79 wt%); consequently, most samples from the Suyunhe plot into the field of high-K calc-alkaline granitoids (Fig. 6). Their A/CNK values mostly range from 0.89 to 1.10, belonging to metaluminous to weakly peraluminous (not shown). It is the widespread sericite alteration that might result in high A/CNK values (even as high as 1.28; Appendix Table 1) in minor samples.

## 5.2. Trace elements of zircon

Analytical data are presented in Table 2 and chondrite-normalized trace element abundances for zircons from three samples are shown in Fig. 6. Although the light rare earth elements (LREE) contents of zircons are relatively scarce compared to those of HREE, REE patterns of zircons from the Suyunhe are all characterized by a steep positive slope from La to Lu with significantly positive Ce anomalies and negative Eu anomalies (Fig. 7).

Generally, the calculation of Ce anomalies is expressed by  $\text{Ce}_{\text{N}}/(\text{La}_{\text{N}} \times \text{Pr}_{\text{N}})^{1/2}$  (where the subscript indicates chondrite normalization). However, the concentrations of La and Pr in a large number of zircons of this study are very low (e.g., ppm levels and even lower) and close to the detection limits of LA-ICP-MS, which may make this calculation of Ce anomalies unreliable. In this study, we therefore employed a  $\text{Ce}^{4+}/\text{Ce}^{3+}$  calculation method proposed by Ballard et al. (2002) on the basis of a lattice-strain model for mineral-melt partitioning of  $\text{Ce}^{4+}$  and  $\text{Ce}^{3+}$  cations. The Eu anomalies ( $\text{Eu}_{\text{N}}/\text{Eu}_{\text{N}*}$ ) were calculated by a conventional method based on chondrite-normalized Sm and Gd contents (where  $\text{Eu}_{\text{N}*} = (\text{Sm}_{\text{N}} \times \text{Gd}_{\text{N}})^{1/2}$ ). The calculated  $\text{Ce}^{4+}/\text{Ce}^{3+}$  values of zircons from three samples show no difference and have a relatively broad range of 5 to 160 (mostly 5–100, average = 35) (Table 2). Similarly,  $\text{Eu}_{\text{N}}/\text{Eu}_{\text{N}*}$  values of zircons are also undistinguishable with a relatively narrow range of 0.2–0.5 (average = 0.3) (Table 2).

## 5.3. Whole rock Sr-Nd isotopes

Sr-Nd isotope analyses for the Suyunhe granitoids are given in Table 3.

Compared to HSE in which measured  $^{87}\text{Rb}/^{86}\text{Sr}$  and  $^{87}\text{Sr}/^{86}\text{Sr}$  ratios are 3.115 to 6.247 and 0.716675 to 0.728855 respectively, those of LSE are much lower (measured  $^{87}\text{Rb}/^{86}\text{Sr} = 0.187$  to 1.707,  $^{87}\text{Sr}/^{86}\text{Sr} = 0.705193$  to 0.711216). Thus, the age-corrected initial  $^{87}\text{Sr}/^{86}\text{Sr}$  ( $I_{\text{sr}}$ ) ratios of LSE are cluster between 0.7041 to 0.7055, which are much higher than those of HSE ranging from 0.7026 to 0.7038 (insert diagram in Fig. 8).

Unlike Rb-Sr isotopic compositions, measured  $^{147}\text{Sm}/^{144}\text{Nd}$  and  $^{143}\text{Nd}/^{144}\text{Nd}$  ratios are indistinguishable and homogeneous, which are 0.1078–0.1494 and 0.512645–0.512828, respectively. Calculated  $\varepsilon_{\text{Nd}}(\text{T})$  values range from +3.5 to +6.4 and the  $T_{2\text{DM}}$  model ages are mostly between 535–774 Ma. In the initial Sr isotopic compositions ( $I_{\text{sr}}$ ) versus  $\varepsilon_{\text{Nd}}$  values diagram (Fig. 8), all samples of the Suyunhe granitoids plot into or near the mantle array, similar to other typical Late Carboniferous–Early Permian juvenile lower crust-derived granitoids found in the West Junggar (Chen and Arakawa, 2005; Geng et al., 2009).

## 6. Discussion

### 6.1. Adakite-like LSE

We noticed the differences of major and trace element concentrations in LSE and HSE in our earliest publication (see Zhong et al., 2015a). Many workers (e.g., Chappell and White, 1992) demonstrated that crystal fractionation can lead to remarkable differences between fractionated rocks and their source rocks, we previously therefore ascribed the compositional differences between LSE and HSE to strong crystal fractionation of ferromagnesian phases and especially plagioclase in HSE (Zhong et al., 2015a; Shen et al., 2017). However, some trace element contents change dramatically from LSE to HSE (e.g., Y and Yb), which could not be explained by the expected fractionation of ferromagnesian phases, e.g., hornblende (which preferentially partitions Y and HREE relative to LREE). We then suspect that the differences between HSE and LSE mainly reflect the distinction of their sources, rather than the degrees of crystal fractionation as previously thought.

To demonstrate this hypothesis, we use several trace element diagrams to examine the evolution trends of LSE and HSE, including Sr/Y vs. Y and La/Yb vs. Yb plots (Fig. 9), trace element Harker diagrams (Fig. 10). Important features of LSE and HSE have been further revealed as follows using the high-quality geochemical database summarized by this article. (1) In the Sr/Y vs. Y diagram (Fig. 9a), the majority of LSE plot within the field of adakitic rocks

**Table 2**

Trace element analyses (ppm) of zircons from the granitoids in the Suyunhe large porphyry Mo deposit.

	ZK0809-3	ZK0809-5	ZK0809-8	ZK0809-12	ZK0809-13	ZK0809-14	ZK0809-17	ZK0809-18	ZK06019-1	ZK06019-2	ZK06019-3	ZK06019-4	ZK06019-5	ZK06019-7	ZK06019-9	ZK06019-10
Ca	4076.74	106.31	221.15	<78.82	<79.36	<86.05	83.36	<77.71	<66.04	<70.16	112.72	<80.16	<73.88	83.41	99.36	<69.34
Cr	<6.01	<5.70	<5.52	<5.72	<5.63	<5.77	<5.47	<5.71	<4.20	<4.26	<4.69	<4.97	<5.22	<4.59	<5.25	<4.86
Mn	18.69	<2.07	<2.09	22.53	<2.19	2.36	<2.05	<2.04	<1.59	2.19	<1.78	<2.00	<1.90	<1.84	6.83	<1.94
Rb	0.607	0.492	0.708	2.32	0.585	0.863	0.559	0.633	0.485	1.297	0.512	0.334	0.634	21.04	1.1	0.805
Sr	4.79	1.139	0.813	0.963	0.56	1.003	0.726	1.055	0.427	1.599	0.535	0.298	0.685	0.866	1.68	0.761
Zr	276619.5	275366	260649	257302.6	265504.8	264466.2	259269.1	267592.8	253437.1	252990.6	260378.6	268441.9	264750.4	239254.8	252287.2	272786.7
Nb	15.87	8.65	13.13	4.38	7.54	4.69	7.73	4.93	3.47	5.04	2.11	1.598	6.53	2.1	13.12	9.2
Cs	<0.241	<0.233	<0.219	<0.226	<0.249	0.347	<0.236	<0.224	<0.179	<0.182	<0.203	<0.223	<0.196	2.86	<0.230	<0.220
Ba	4.98	0.74	<0.39	2.5	<0.25	2.72	0.38	<0.38	<0.232	4.25	0.45	<0.41	<0.253	2.11	0.52	<0.41
La	12.98	2.64	0.9	0.371	<0.085	0.25	0.189	3.79	0.2	0.419	0.275	<0.073	3	0.071	12.75	1.124
Ce	71.27	34.23	22	19.8	26.51	11.57	17.41	52.38	21.7	35.95	15.68	13.97	42.67	10.48	120.26	32.15
Pr	6.99	2.16	0.767	0.641	0.17	0.131	0.471	4.62	0.5	0.846	0.252	<0.045	3.14	0.168	11.27	1.435
Nd	34.69	11.61	7.48	4.95	1.45	0.93	4.84	24.78	4.9	7.82	3.16	0.47	20.19	2.55	74.75	11.25
Sm	16.88	7.32	9.32	6.52	3.03	1.4	6.35	11.69	5.98	7.1	5.78	1.54	10.54	3.96	34.82	9.44
Eu	1.65	1.35	3.12	1.7	0.464	0.362	2.08	2.68	0.778	1.88	1.82	0.342	1.56	1.388	4.09	1.51
Gd	33.54	23.22	39.79	25.62	18.97	7.33	27.84	37.81	23.03	32.13	28.22	8.63	31.58	19.22	60.79	32.46
Tb	11	8.37	13.53	9.3	8.23	3.37	9.83	12.39	8.74	12.12	10.14	3.51	11.15	6.61	17.75	12.23
Dy	134.18	101.74	155.3	111.78	113.34	47.15	117.32	144.34	109.05	154.12	121.47	48.41	140.52	78.45	208.14	157.26
Ho	51.79	40.88	58.48	43.17	48.3	21.07	45.49	55.16	44.3	63	47.02	20.51	58.25	30.18	82.73	65.42
Er	251.98	199	266.84	207.37	242.77	111	215.39	260.58	216.22	305.05	216.7	105.17	289.85	141.55	390.94	322.47
Tm	62.09	47.66	60.48	48.23	59.82	28.67	50.62	60.35	52.1	73.01	49.74	25.66	70.48	32.44	91.6	78.66
Yb	678.31	514.68	630.38	510.07	646.68	326.62	544.25	642.77	562.15	795.96	522.28	282.56	770.26	345.11	972.91	848.5
Lu	131.51	101.4	122.05	100.94	128.64	67.32	106.24	125.9	106.62	154.4	101.75	56.33	151.1	67.17	185.86	162.69
Y	1641.98	1292.72	1837.17	1359.01	1536	681.23	1464.5	1774.52	1397.1	2032.8	1430.52	644.71	1901.46	915.12	2657.65	2089.48
Hf	10848.98	9429.77	8261.19	8091.24	10323.42	11153.13	8520.1	8799.94	9746.07	8673.82	8540.78	9843.79	11350.43	7353.45	10329.11	10725.83
Ta	1.853	1.071	0.461	0.546	2.69	1.142	0.479	1.361	1.063	1.653	0.458	0.676	2.305	0.341	3	2.389
Th	309.24	196.25	228.34	163.9	381.95	97.96	193.49	258.52	235.65	409.46	180.78	71.8	367.17	91.08	672.9	488.01
U	760.97	422.59	316.43	271.34	918.51	340.42	336.39	517.12	582.78	849.6	316.07	182.89	1023.64	144.39	1466.39	1453.18
Eu <sub>N</sub> /Eu <sub>N*</sub>	0.21	0.32	0.50	0.40	0.19	0.35	0.48	0.39	0.20	0.38	0.44	0.29	0.26	0.49	0.27	0.26
Ce <sup>4+</sup> /Ce <sup>3+</sup>	5	10	13	21	131	46	26	8	42	38	32	160	11	44	7	18
	ZK6019-11	ZK6019-12	ZK6019-15	ZK6019-16	ZK6019-19	ZK6019-20	ZK9235-1	ZK9235-2	ZK9235-6	ZK9235-7	ZK9235-11	ZK9235-12	ZK9235-14	ZK9235-15	ZK9235-17	ZK9235-21
Ca	<70.24	<80.07	<73.14	<83.54	171.52	<82.02	3786.57	95.31	237.06	759.23	1266.51	<74.86	151.57	783.01	<77.67	215.37
Cr	<5.03	<4.63	<5.05	<5.05	<4.94	<5.17	<4.97	<4.58	<5.36	17.48	<5.19	<4.69	<4.65	<4.84	<4.89	<4.56
Mn	<2.00	<1.89	<2.02	<2.08	<1.91	13.01	19.39	17.45	79.11	109.27	7.19	<1.87	<1.89	7.14	<1.87	<1.80
Rb	0.425	0.391	0.692	0.586	0.48	2.49	1.22	20.02	0.852	0.605	0.924	0.676	13.11	0.72	0.634	0.343
Sr	0.409	0.456	0.376	0.551	0.592	0.411	4.89	1.007	1.255	2.22	1.94	0.539	1.87	1.178	0.797	0.526
Zr	269361.5	266424.7	266490.1	266104.2	263202	257157.6	262058	258315.3	258253.7	257874	267975	260796.8	240628.5	264987.9	267900.6	279558.1
Nb	10.31	5.99	0.791	8.09	6.26	3.37	1.86	6.98	5.85	9.29	14.88	2.46	6.98	6.3	12.1	3.3
Cs	<0.228	<0.221	<0.217	<0.23	<0.210	<0.231	0.663	5.07	<0.237	<0.209	<0.224	<0.201	3.69	<0.214	<0.216	<0.203
Ba	<0.33	<0.31	0.47	<0.41	<0.37	2.56	2.42	1.79	2.07	0.46	<0.30	0.48	4.07	0.67	<0.37	<0.24
La	0.332	0.965	<0.071	1.31	0.76	0.122	10.15	0.387	4.38	9.19	6.13	<0.067	0.631	3.97	0.381	1.473
Ce	24.15	28.77	12.34	32.83	33.31	16.99	42.44	27.36	39.18	53.1	62.33	24.2	24.72	31.4	18.97	24.79
Pr	0.412	1.58	0.11	1.643	0.628	0.104	3.8	0.511	2.16	3.9	3.58	0.251	0.868	1.759	0.479	0.734
Nd	3.27	12.43	1.71	12.55	4.43	1.5	19.4	4.8	13.36	19.22	22.24	4	8.73	9.52	3.16	4.48
Sm	3.82	7.42	3.4	8.95	3.72	3.17	7.51	6	8.47	7.73	13.85	7.16	11.19	5.35	3.43	3.06
Eu	0.521	0.653	0.999	1.37	0.625	0.697	1.34	1.63	2.28	1.88	1.313	2.27	2.79	0.848	0.411	0.569
Gd	16.48	17.42	17.31	32.85	17.89	18.4	22.85	25.3	29.11	21.83	39.06	33.2	44.57	21.76	16.07	14.28
Tb	6.55	6.15	6.14	11.42	7.03	7.56	7.78	9.3	10.63	7.96	14.34	11.93	14.94	8.91	7.05	5.49
Dy	86.24	79.29	74.09	144.45	93.99	96.19	94.92	113.03	132.7	103.84	182.26	143.33	169.26	118.05	99.91	72.46
Ho	36.26	33.8	29.5	57.42	39.84	39.06	38.31	45.37	53.21	44.87	77.27	56.24	62.37	50.61	46.3	30.58
Er	177.12	170.99	140.2	263.92	198.04	184.07	184.54	217.76	258.7	229.59	388.76	268.65	271.53	254.6	248.34	151.12
Tm	42.33	42.55	32.96	58.87	47.95	42.53	44.19	51.61	60.94	57.95	95.08	63.56	58.34	62.25	64.77	36.16
Yb	450.66	469.36	354.89	596.28	524.76	437.69	477.22	549.98	651.44	659.05	1052.68	678.7	580.41	686.5	745.75	387.95
Lu	86.87	92.56	69.47	110.12	102.33	81.45	94.08	109.02	125.94	131.61	205.8	131.99	106.12	134.68	152.33	74.83
Y	1104.65	1059.34	898.6	1724.42	1259.85	1186.96	1166.6	1419.67	1689.99	1474.46	2540.98	1788.7	1825.55	1620.13	1521.25	944.14
Hf	10018.71	10865.4	9322.87	8333.57	10757.7	9181.14	9673.86	8795.88	8715.33	11444.57	10744.5	8997.47	7919.1	11273.33	11614.06	10478.56
Ta	1.649	2.039	0.355	1.748	2.383	0.975	0.779	1.023	1.475	2.279	3.75	0.849	0.605	2.257	2.64	1.156
Th	145.87	193.96	105.39	326.93	584.08	120.35	183.54	284.97	332.09	326.22	657.55	260.35	165.38	318.63	354.79	183.85
U	346.57	603.78	187.24	658.65	1218.27	264.51	413.35	481.29	644	1007.91	1772.01	483.24	278.75	959.82	1310.71	411
Eu <sub>N</sub> /Eu <sub>N*</sub>	0.20	0.18	0.40	0.24	0.23	0.28	0.31	0.40	0.44	0.44	0.17	0.45	0.38	0.24	0.17	0.26
Ce <sup>4+</sup> /Ce <sup>3+</sup>	48	17	68	15	39	86	6	37	9	8	11	80	1			

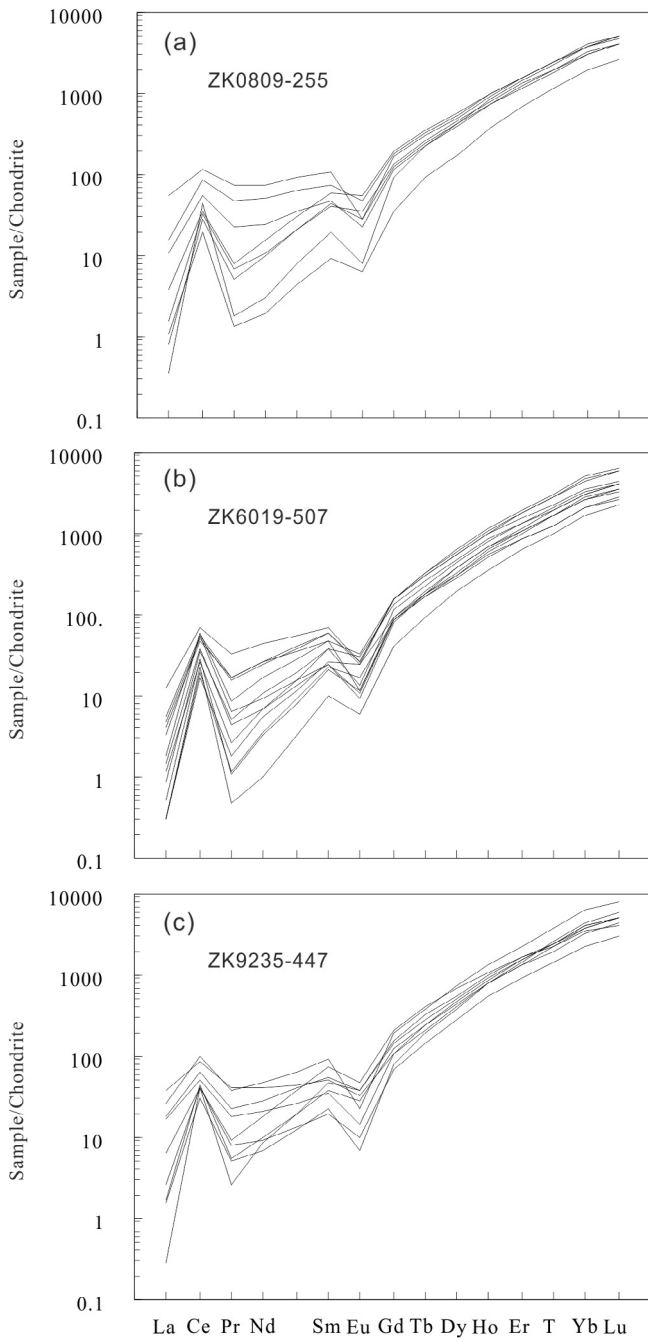


**Fig. 7.** Chondrite-normalized REE diagrams of zircons from the granitoids in the Suyunhe large porphyry Mo deposit. The normalization values are from Sun and McDonough (1989).

attributed to their high Sr contents (mostly 251–574 ppm), low Y contents (mostly 8.0–17.5 ppm) and thus high Sr/Y ratios (mostly >20), whereas most HSE plot into the normal arc andesite, dacite and rhyolite lavas (ADR) field with lower Sr contents (mostly 14.9–141.0 ppm), higher Y contents (9.16–34.7 ppm) as well as lower Sr/Y ratios (1.2–9.5). (2) In the Yb-La/Yb diagram (Fig. 9b), although all the samples plot into the ADR field according to the strict parameter proposed by Defant and Drummond (1993) and Richards and Kerrich (2007), it is still easy to find that LSE commonly show lower Yb (0.9–1.9 ppm) (Fig. 10d) and higher La/Yb ratios (6.1–17.1) than HSE (Yb = 1.5–4.6 ppm; La/Yb = 1.5–10.4); moreover, if we take a more permissive criteria for adakites (La/

$\text{Yb} \geq 8$ ; see Sajona et al., 1993; Richards and Kerrich, 2007; Castillo, 2012; and references therein), most LSE still plot into the adakite field in the Yb-La/Yb diagram (Fig. 9b), whereas HSE plot into the ADR field. (3) Sr contents keep constant in LSE whereas significantly decrease in HSE with increasing  $\text{SiO}_2$  (Fig. 10a); differently, although Y is highly scattered with increasing  $\text{SiO}_2$  in both cases (Fig. 10b), a sharply increase at ~75 wt.%  $\text{SiO}_2$  render Sr/Y ratios much lower in HSE than those in LSE (Fig. 10c). (4) Similar to Y contents, the variation of Yb with  $\text{SiO}_2$  is also rather scattered (Fig. 10e), but a dramatic increase from LSE to HSE is clearly manifested; La is only highly scared in LSE whereas a smooth descending trend is exhibited in HSE (Fig. 10d), which results in an evident decrease of La/Yb ratios in HSE (Fig. 10f). (5) Controlled by variations of Sr-Y and La-Yb, HSE show consistent decreasing trends of Sr/Y and La/Yb ratios with increasing  $\text{SiO}_2$ , whereas these ratios are highly scattered in LSE (Fig. 10c and f). In conclusion, all these variation diagrams, combined with high MgO (0.52–1.32 wt.%) and Mg# (0.32–0.52; mostly >0.4) in LSE, firmly confirm adakite-like features of LSE (e.g., Defant and Drummond, 1993; Bourdon et al., 2002; Castillo, 2006; Richards and Kerrich, 2007; Richards et al., 2012). Besides, they imply that HSE could not be simply derived from further fractionation of magmas of LSE; rather, these geochemical characteristics argue the existence of two different magmas sources (see 6.2 for further discussions).

## 6.2. Petrogenesis

### 6.2.1. LSE: Partial melting of thickened juvenile lower crust

Although Richards and Kerrich (2007) argued that many rocks, only fitting to some of the criteria of adakites (which then are referred to as adakite-like rocks), are virtually not adakites, many workers however have demonstrated that adakite-like rocks and adakites share similar origins and magmatic evolution processes. Several petrogenetic models have been proposed for origins of adakites and/or adakite-like rocks, including (1) assimilation-fractional crystallization (AFC) processes from parental basaltic magmas (e.g., Castillo et al., 1999; Macpherson et al., 2006; Li et al., 2009), (2) magma mixing between felsic and basaltic magmas (e.g., Richards and Kerrich, 2007; Streck et al., 2007), (3) partial melting of young and hot subducted oceanic slabs (e.g., Defant and Drummond, 1993; Rapp et al., 1999; Tang et al., 2010), (4) partial melting of delaminated lower crust (e.g., Kay and Mahlburg, 1993; Xu et al., 2002; Wang et al., 2006b), (5) partial melting of subducted continental crust (e.g., Wang et al., 2008; Qin et al., 2010), and (6) partial melting of thickened lower crust (e.g., Atherton and Petford, 1993; Wang et al., 2005; Hou et al., 2013; Long et al., 2015; Zhang et al., 2016). We consider these alternative processes in the following sections with specific reference to the adakite-like LSE in the Suyunhe large porphyry Mo deposit.

The first two models (i.e., AFC and magma mixing between felsic and basaltic magmas) can be firmly precluded based on the following evidence. (1) Straight arrays in binary plots should have been displayed if crystal fractionation and/or magmas mixing occurred (Macpherson et al., 2006; Zhang et al., 2016); however, most trace elements (e.g., Sr, Y, La, Yb) of LSE are extremely scattered with increasing  $\text{SiO}_2$  (Fig. 10a–b, d–e). (2) In  $\text{SiO}_2$  versus  $\varepsilon\text{Nd}$  and  $^{87}\text{Sr}/^{86}\text{Sr}$  diagrams (Fig. 11a and b), linear trends of  $\varepsilon\text{Nd}$  and  $^{87}\text{Sr}/^{86}\text{Sr}$  with increasing  $\text{SiO}_2$  are not displayed (Fig. 11a and b), precluding the existence of crustal contamination (and thus AFC processes) (Tang et al., 2010; Hou et al., 2013). (3) Candidates for mantle-derived basaltic and crust-derived felsic end-members in the West Junggar are most plausibly represented by the Kexia basalts (~345 Ma; average = +7.9) and the Miaoergou granites

**Table 3**

Sr-Nd isotopic analyses of the granitoids from the Suyunhe large porphyry Mo deposit.

Sample No.	Stock	Rock	Rb [ppm]	Sr [ppm]	Sm [ppm]	Nd [ppm]	$^{87}\text{Rb}/^{86}\text{Sr}$	$^{87}\text{Sr}/^{86}\text{Sr}$	$^{147}\text{Sm}/^{144}\text{Nd}$	$^{143}\text{Nd}/^{144}\text{Nd}$	$I_{\text{Sr}}$	$T_{\text{2DM}}(\text{Ma})$	$\epsilon\text{Nd(T)}$	Data sources
SIM2-1	I	MGP	146.5	136.2	2.44	11.06	3.115	0.716675	0.1334	0.512822	0.70360	570	6.0	This article
s1p3-1	I	GDP	68.3	68.3	2.27	11.19	1.099	0.708847	0.1228	0.512748	0.70424	656	4.9	
zk0809-166	I	MGP	163.8	76.08	1.67	8.23	6.247	0.728855	0.1230	0.512817	0.70263	547	6.3	
zk0809-193	I	GDP	141.8	240.5	4.46	21.59	1.707	0.711216	0.1251	0.512828	0.70405	535	6.4	
zk5219-474	II	MGP	160.0	89.58	2.70	10.96	5.180	0.725424	0.1494	0.512799	0.70368	656	4.9	
zk6-19-490	II	GP	203.8	119.9	2.02	10.05	4.928	0.724111	0.1219	0.512790	0.70342	587	5.8	
zk6019-507	II	GP	160.3	111.3	3.27	15.32	4.172	0.721178	0.1294	0.512800	0.70367	594	5.7	
zk9235-457	III	G	149.7	114.7	3.02	14.94	3.781	0.719404	0.1223	0.512758	0.70353	638	5.1	
s3d1-1	III	TP	44.4	686.0	3.26	17.84	0.187	0.705193	0.1106	0.512740	0.70441	632	5.2	
s3d4-3	III	TP	50.9	567.7	2.93	15.95	0.259	0.705226	0.1111	0.512770	0.70414	584	5.8	
S-12**	I	MGP?	117.0	346.0	1.44	6.31	0.978	0.708309	0.1380	0.512813	0.70420	599	5.6	Yang et al. (2015)
S-16**	I	MGP?	139.0	377.0	2.55	14.30	1.067	0.710002	0.1078	0.512645	0.70552	774	3.5	
S-19**	I	MGP?	151.0	383.0	3.22	16.20	1.142	0.709220	0.1202	0.512743	0.70442	656	4.9	
S-21**	I	MGP?	122.0	293.0	2.28	12.00	1.205	0.709347	0.1149	0.512797	0.70429	553	6.2	
ZK0003-215*	I	MGP	152	73	2.66	12	6.0241	0.728811	0.1345	0.512749	0.70352	690	4.5	Shen et al. (2013a)
ZK0003-221*	I	MGP	171	123	2.48	11.7	4.0321	0.719778	0.128	0.512763	0.70285	648	5.0	
zk5219-429	II	MGP	153.8	112.1	2.87	12.82	3.977	0.720491	0.1356	0.512748	0.70380	695	4.5	Shen et al. (2017)
zk9235-447	III	MGP	159.9	118.8	2.96	13.50	3.900	0.719825	0.1325	0.512819	0.70345	573	5.9	
SYP9-2	III	TP	62.0	510.0	2.86	15.60	0.352	0.705768	0.1111	0.512667	0.70429	749	3.8	
SYP9-3	III	TP	62.0	514.0	3.00	16.30	0.350	0.705565	0.1111	0.512702	0.70410	693	4.5	

T = 295 Ma, the emplacement age of the Suyunhe granitoids.

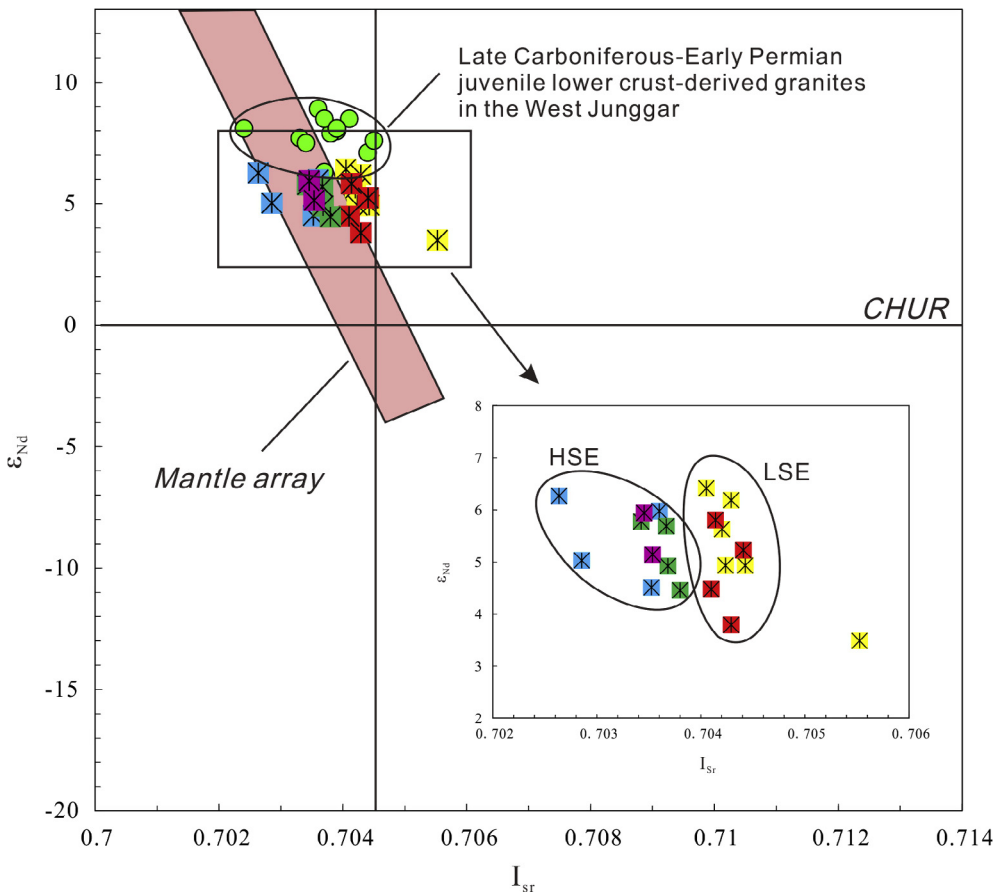


**Fig. 8.** Plot of initial Sr isotopic compositions ( $I_{\text{Sr}}$ ) vs.  $\varepsilon_{\text{Nd}}$  values of the granitoids in the Suyunhe large porphyry Mo deposit. Symbols are as in Fig. 3. The field for the mantle array is modified after Chen and Arakawa (2005). The isotopic data for the Late Carboniferous–Early Permian juvenile lower crust-derived granitoids in the West Junggar are from Chen and Arakawa (2005) and Geng et al. (2009). The inset diagram clearly shows that LSE have much higher initial  $\text{Sr}^{87}/\text{Sr}^{86}$  than HSE, although their  $\varepsilon_{\text{Nd}}$  ratios are indistinguishable.

(~290 Ma; average  $\varepsilon_{\text{Nd}} = +7.2$ ) (Tang et al., 2010 and references therein); LSE from the Suyunhe deposit have noticeably lower  $\varepsilon_{\text{Nd}}$  values (+3.9 to +6.5) than those two magma end-members, suggesting that they are not produced by magma mixing. Besides, AFC and magma mixing between felsic and basaltic magmas are also inconsistent with the petrographic evidence. Generally, AFC and magma mixing should be accompanied by mafic xenoliths/enclaves, mingling textures, and contemporary basaltic to intermediate rocks (Richards and Kerrich, 2007; Tang et al., 2010; Zhang et al., 2016), all of which are absent in the Suyunhe deposit.

Adakites and adakite-like rocks derived from melting of oceanic slab or delaminated lower crust generally have extremely high Mg# (normally >40) and Ni (>20 ppm) values attributed to reacting with the peridotitic asthenospheric mantle wedge during ascent of slab melts (Stern and Kilian, 1996; Rapp et al., 1999; Prouteau et al., 2001; Richards and Kerrich, 2007; Zhang et al., 2016; and references therein). In Fig. 3, LSE from the Suyunhe deposit exhibit relatively low MgO contents and Mg# values that are similar to, or only slightly higher than, those of experimental melts from metabasalts and eclogite (Rapp and Watson, 1995; Rapp et al., 1999); besides, LSE also have lower Ni contents (2.3–14.7 ppm, average = 6.3 ppm) than oceanic slab- or delaminated lower crust-derived adakitic rocks and much higher Rb/Sr ratios (0.1–1.0) than those (<0.05) of slab-derived adakites (Huang et al., 2009). In addition, the granitoids in the Suyunhe deposits are believed to come from an arc setting (Yang et al., 2015; Zhong

et al., 2015a) or at the early stage of syn-collision (Shen et al., 2017), and therefore are inconsistent with delamination of thickened lower crust [which generally occurs in a post-collisional extension setting (Zhang et al., 2016 and references therein)]. Moreover, adakitic rocks generated by delaminated lower crust should have negative  $\varepsilon_{\text{Nd}}$  values (e.g., Xu et al., 2002; Qin et al., 2010), whereas LSE in the Suyunhe deposit have much higher  $\varepsilon_{\text{Nd}}$  values (+3.9 to +6.5). Although continental crust subduction could occur in a syn-collisional setting, adakitic rocks generated by this mechanism should also be characterized by low  $\varepsilon_{\text{Nd}}$  values (generally <-3) (Tang et al., 2010 and references therein). Collectively, we suggest that adakite-like LSE in the Suyunhe deposit are unlikely to have been derived from partial melting of oceanic slab, or delaminated lower crust, or subducted continental crust.

Thickened lower crust is the last candidate for LSE in the Suyunhe deposit. In Fig. 3, the Mg# and MgO values of LSE are consistent with those of adakites derived from thickened lower crust, supporting that LSE might be generated by thickened lower crust. Besides, LSE show relatively uniform, depleted Sr-Nd isotopic characteristics ( $\varepsilon_{\text{Nd}}(T) = +3.5\text{--}+6.4$  and  $I_{\text{Sr}} = 0.7041\text{--}0.7055$ ), which are similar to juvenile lower crust-derived granitoids in the West Junggar (e.g., the Miaoergou batholith, Geng et al., 2009). The young Nd model ages (535 Ma to 774 Ma) also match the time span when the juvenile crust formed in this area (Chen and Jahn, 2004; Chen and Arakawa, 2005). Collectively, we argue that adakite-like LSE from the Suyunhe granites possibly formed by partial melting of

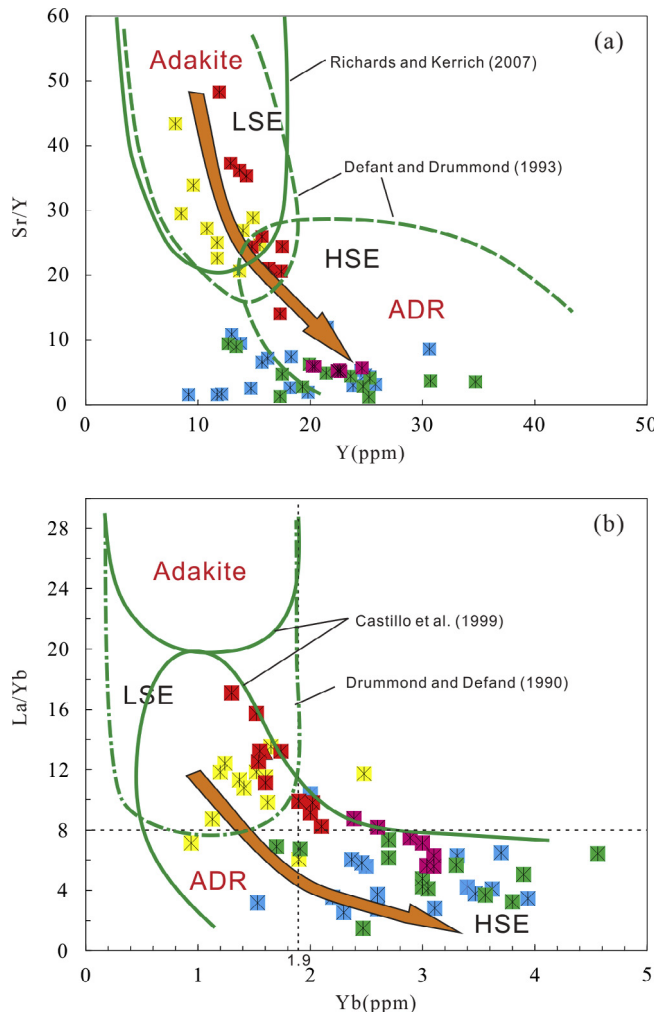


**Fig. 9.** Y versus Sr/Y (a), and Yb versus La/Yb (b) diagrams. Symbols are as in Fig. 3.

thickened juvenile lower crust. Since the scarred evolution trends of Y and Yb with increasing SiO<sub>2</sub> in LSE exclude significant amphibole ( $\pm$ garnet) fractionation processes, the partial melting of the thickened lower crust needs to leave a garnet  $\pm$  amphibole residue (which preferentially partitions Y and HREE relative to LREE and thus renders the HREE depleted in the melts) (e.g., Martin et al., 2005) to form the adakite-like features of LSE (e.g., high Sr/Y and La/Yb ratios). In West Junggar, adakites are also found in the Baogutu area. However, they were considered to be derived from partial melting of subducted oceanic crust (Geng et al., 2009; Tang et al., 2010), thus different from HSE in the Suyunhe deposit.

#### 6.2.2. HSE: Partial melting of shallower juvenile lower crust +plagioclase-dominated fractionation

Strong depletions in some trace elements, such as Ba, Sr, P, Ti and Eu, and good covariation between some major/trace elements and SiO<sub>2</sub> demonstrate an advanced fractional crystallization during the formation of HSE. Particularly, pronounced Eu depletion, as well as the negative correction of Sr, Al<sub>2</sub>O<sub>3</sub> with increasing SiO<sub>2</sub> (not shown), emphasizes dominant fractionation of plagioclase, as proposed by the early publications with regard to the Suyunhe granitoids (Zhong et al., 2015a; Shen et al., 2017), and/or a plagioclase residue in the source; depletion in Nb-Ta-Ti and P (Fig. 4b) probably resulted from the separation of Ti-bearing phases (such as ilmenite and titanite; Green, 1994) and apatite, respectively;

the negative correlations of FeO, MgO and CaO with SiO<sub>2</sub> (not shown), however, might indicate minor fractionation of ferromagnesian phases. La contents also decrease with increasing SiO<sub>2</sub> (Fig. 10d), which might indicate minor allanite fractionation. Besides, HSE are characterized by much lower Sr/Y and La/Yb ratios. All these characteristics are noticeably different from those of LSE. However, the uniform, depleted Sr-Nd isotopic characteristics ( $\varepsilon$ Nd(T) = +5.6–+6.5, and  $I_{\text{Sr}} = 0.7026$ –0.7038) and young Nd model ages (547–695 Ma) of HSE also indicate a source of juvenile lower crust, just like that of LSE.

A good petrogenesis model for HSE should explain the above features. Fractional crystallization of plagioclase (which preferentially partitions Sr) in the absence of garnet  $\pm$  amphibole can lower Sr/Y ratios, therefore erasing the adakitic features (Sun et al., 2012, 2013). This mechanism seems to support a hypothesis that HSE are evolved from LSE by plagioclase-dominated fractionation, considering that Sr and Sr/Y values decrease with increasing SiO<sub>2</sub> in HSE. However, plagioclase fractionation could not explain the sharp variations of Sr, Y and Yb at  $\sim$ 75 wt% SiO<sub>2</sub> in HSE (Fig. 10a–b, and e). Thus, although crystal fractionation processes are confirmed in HSE, it cannot be the key mechanism to result in the distinctions between LSE and HSE. This is also demonstrated by the Sr isotopic evidence where LSE show much higher initial  $^{87}\text{Sr}/^{86}\text{Sr}$  values than HSE (insert diagram in Fig. 8), although their  $\varepsilon$ Nd values are similar. The hydrothermal alteration can also render the increase of initial  $^{87}\text{Sr}/^{86}\text{Sr}$  values, and Hou et al. (2012) proposed that this could be evaluated by the LOI values versus initial  $^{87}\text{Sr}/^{86}\text{Sr}$  values plot, in which  $^{87}\text{Sr}/^{86}\text{Sr}$  values will increase with LOI values if hydrothermal alteration exists. However, neither HSE nor LSE from the Suyunhe deposit display this trend (Fig. 11c), excluding the influences from hydrothermal alteration. Therefore, we argue again that those differences between LSE and HSE mainly reflect the discrepancy of their sources.

The sharp increase of Y and Yb at  $\sim$ 75 wt% SiO<sub>2</sub> (Fig. 10b and e) and the much higher HREE contents in HSE imply that to generate HSE, a residual phase of amphibole  $\pm$  garnet could not exist. However, a plagioclase residue is needed to explain the sharp decrease of Sr contents at  $\sim$ 75 wt% SiO<sub>2</sub> (Fig. 10a). Experimental data have reflected that melt compositions formed by partial melting of basaltic rocks are predominantly dependent on the pressure (and thus the depth) of melting (Rapp and Watson, 1995; Rapp et al., 1999; Xiong et al., 2005). Granitic melts at pressures of below 1 GPa are normally in equilibrium with a plagioclase residue, whereas those at pressures of higher than  $\sim$ 1.2 GPa are in equilibrium with a garnet-rich residue (Zhang et al., 2010b; Xie et al., 2011; and references therein). Therefore, we suggest that HSE in the Suyunhe deposit were formed by initial melting of juvenile crust at pressures of less than 1 GPa, i.e., at depths of  $<\sim$ 33 km using a pressure gradient of 30 MPa/km, whereas that to produce the parental magmas of LSE probably happened at pressures of  $>1.2$  GPa and thus at depths of  $>40$  km where the crust was thickened. This finding is consistent with the previous research that argued the granitoids in the Suyunhe deposits were formed by sources at different depths (Shen et al., 2017). Similar circumstances could also be found in the Middle-Lower Yangtze River Valley metallogenic belt, one of the most important porphyry-skarn and skarn Cu-Fe-Au-W-Mo belts in China. In this belt, there are two episodes of intrusions: 140–136 Ma diorites and quartz diorites that are related to skarn Cu-Fe or Fe-Cu deposits and 133–127 Ma quartz diorites and granites that are related to skarn Fe deposits (Xie et al., 2011). The former displays adakitic geochemical features and is believed to be in equilibrium with a garnet-rich residue, whereas the latter is different from adakitic rocks and in equilibrium with a plagioclase residue (Xie et al., 2011).

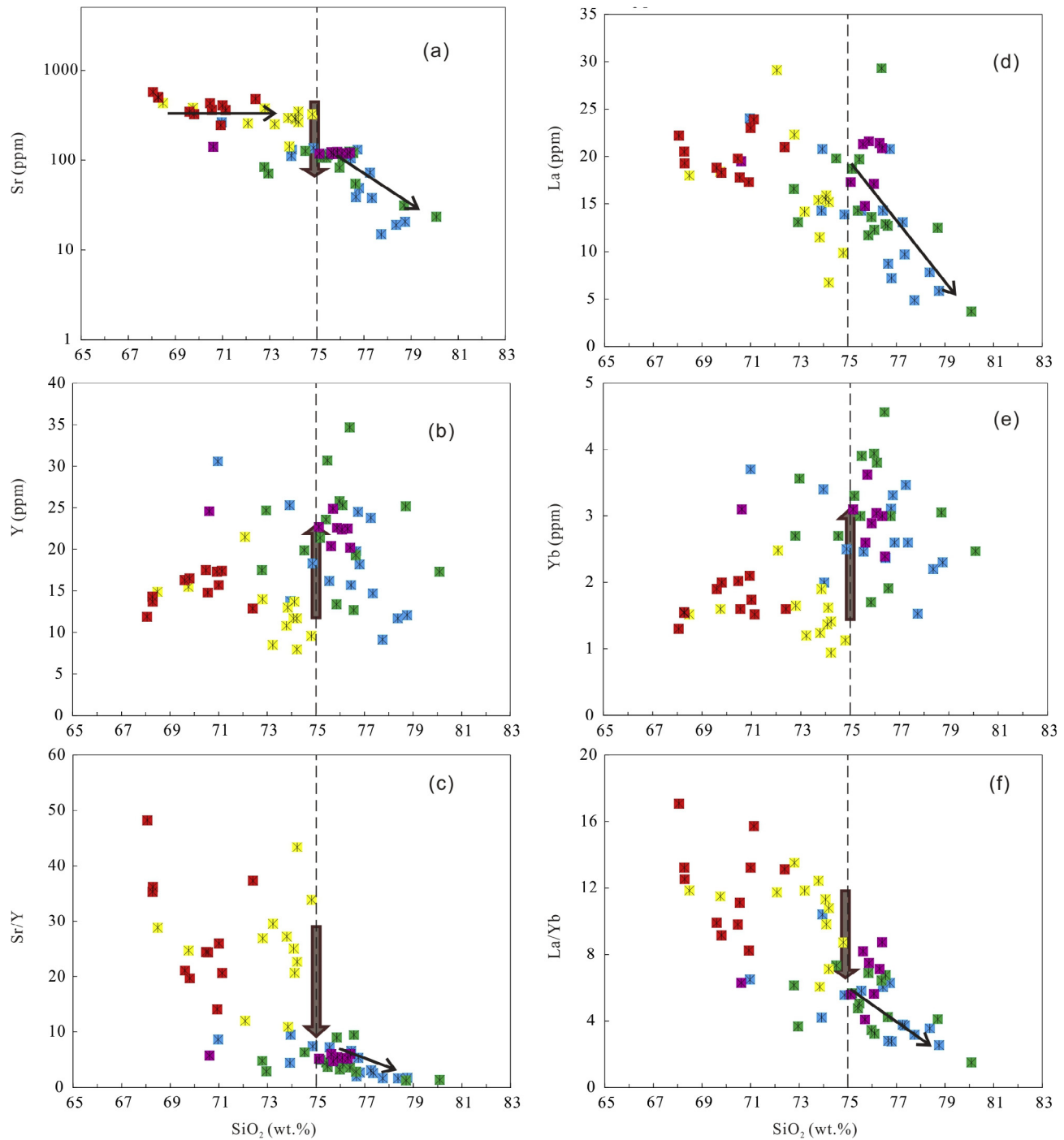


**Fig. 10.** Harker diagrams of the granitoids from the Suyunhe large porphyry Mo deposit. Symbols are as in Fig. 3.

### 6.3. Geodynamic setting

The Late Carboniferous–Early Permian tectonic-magmatic evolution of the West Junggar has long been debated. Two distinct, competing viewpoints emphasize either a subducted model (Geng et al., 2009; Liu et al., 2009; Tang et al., 2010, 2012b,c; Yin et al., 2010, 2013; Shen et al., 2013b) or a post-collisional model (Chen and Jahn, 2004; Chen et al., 2010; Xu et al., 2012). Our new data, combined with an integrative analysis of previous published data with regard to Late Paleozoic tectonic-magmatic suites

in the West Junggar, provide new constraints on the Late Carboniferous–Early Permian tectonic-magmatic evolution of the Suyunhe porphyry Mo deposit.

The post-collisional model was accepted mainly due to the ages of ophiolites that were dominantly Cambrian to Early Carboniferous in ages (Zhang and Huang, 1992; Liu et al., 2009; Chen and Guo, 2010; Zhang et al., 2010a; Yang et al., 2012a, 2012b, 2013; Zhao et al., 2013; Wen et al., 2016; Weng et al., 2016), as well as those of I-type and A-type granitoids with undeformed and alkali-enriched features (Chen and Jahn, 2004; Chen et al., 2010;

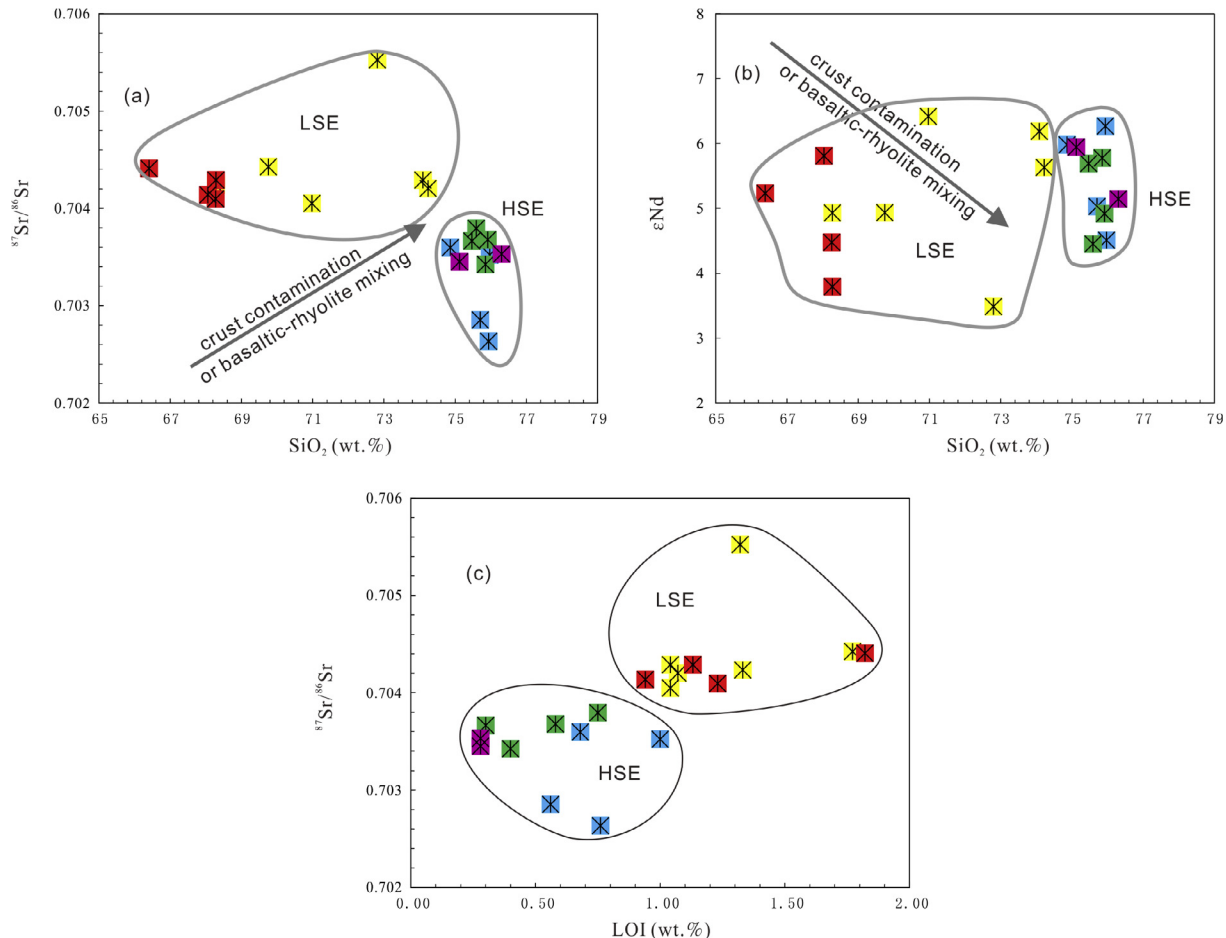


**Fig. 11.**  $\text{SiO}_2$  versus  $\epsilon_{\text{Nd}}$  (a);  $\text{SiO}_2$  versus  $^{87}\text{Sr}/^{86}\text{Sr}$  (b); and LOI versus  $^{87}\text{Sr}/^{86}\text{Sr}$  (c). Symbols are as in Fig. 3.

Xu et al., 2012). However, Liu et al. (2009) reported a U–Pb age of  $302 \pm 1.7$  Ma for the E-MORB-type mafic rocks from the Darbut ophiolite in the West Junggar, indicating that the Junggar oceanic basin might still exist in Late Carboniferous. Moreover, increasing evidence confirmed the existence of subduction during Late Carboniferous to Early Permian because of the discoveries of large numbers of  $\sim 320$ – $\sim 300$  Ma arc- and/or ridge subduction-related granitoids (e.g., Geng et al., 2009; Tang et al., 2010, 2012b,c; Yin et al., 2010; Shen et al., 2013b), as well as innumerable 297– $\sim 284$  Ma magnesian and dioritic dikes (Yin et al., 2013, 2015a). Besides, some  $\sim 300$  Ma granites in the West Junggar that were previously believed to be typical of post-collisional magmatic intrusions (e.g., the Miaoergou and Kalamay suites; Chen and Arakawa, 2005), were recently confirmed to form in a subducted environment (Geng et al., 2009; Tang et al., 2010). Thus, it is quite possible that subduction in the West Junggar lasted at least into Late Carboniferous ( $\sim 300$  Ma) or even later.

Based on the chronological results and the above evidence, Yang et al. (2015) and Zhong et al. (2015a) argued that granitoids in the Suyunhe deposit formed in a subducted environment. However, Shen et al. (2017) proposed that these granitoids were generated in a syn-collisional environment mainly based on their newly dating results that implied the granitoids in the Suyunhe formed at  $\sim 294$  Ma. Nevertheless, a post-collisional setting for the Suyunhe granitoids could be firmly precluded. If LSE and HSE did not form in a subducted setting as suggested by Yang et al. (2015), then they

most probably formed at the beginning stage of collision (and thus the syn-collisional stage) of Yili and Junggar terranes as suggested by Shen et al. (2017). More chronological evidence is still needed to test which one of these hypotheses is more likely. For this article, however, both of them are acceptable because the juvenile lower crust under the Suyunhe deposit could be thickened in the late subduction or at the start of the syn-collision (Richards and Kerrich, 2007; and references therein).

The closely temporal and spatial relationships of LSE and HSE imply that initial melting of their sources is probably triggered simultaneously and by same exotic heat sources. Generally, these heat sources are related to basaltic magma underplating during asthenosphere upwelling initiated by delamination of thickened lower crust, by ocean ridge subduction, or by a slab rollback (Zhang et al., 2016; and reference therein). The delamination of thickened lower crust could be excluded because the Suyunhe granites formed in a subducted or syn-collisional environment as discussed before, rather than in a continental post-collisional setting. Oceanic ridge subduction is always associated with high temperature magmatism (Geng et al., 2009), whereas the Suyunhe granites are typical of low temperature intrusions ( $650$ – $750$  °C; Zhong et al., 2015a). Thus, the only possible heat source that triggered the partial melting of (thickened) juvenile lower crust was related to asthenosphere upwelling subsequent to a slab rollback event, similar to that found in the Central Tianshan block (Zhang et al., 2016).

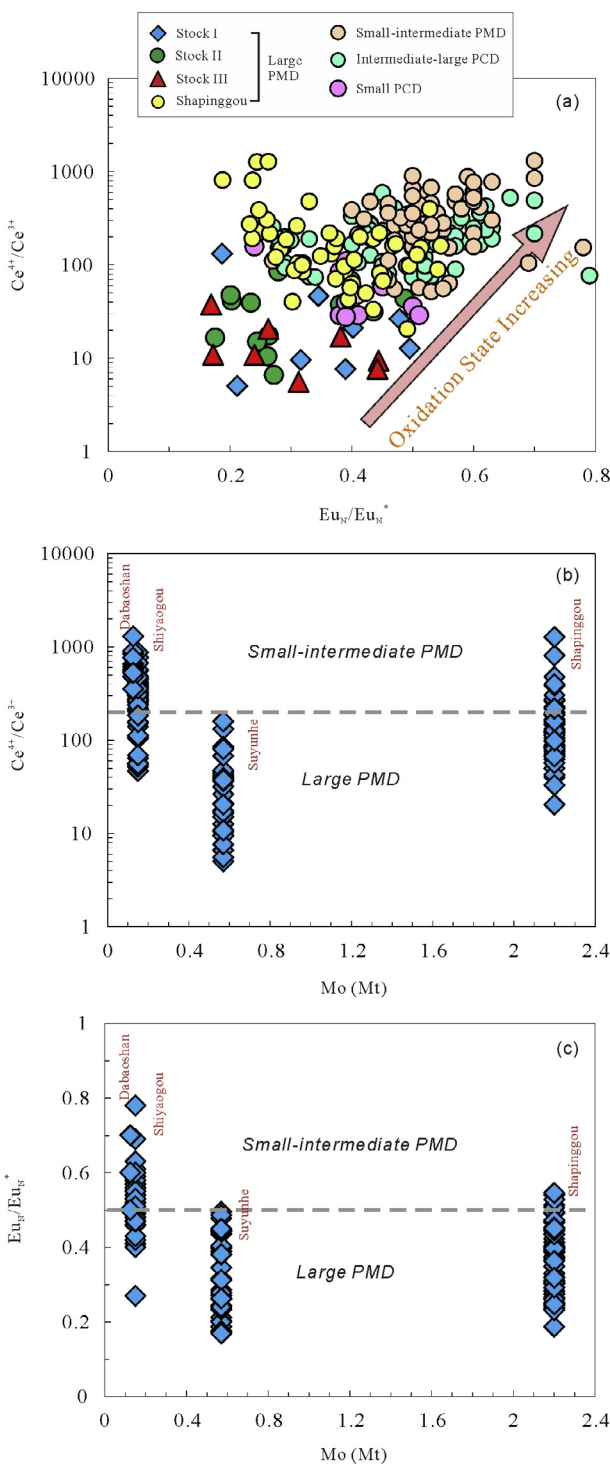


**Fig. 12.** (a)  $\text{Eu}_{\text{N}}/\text{Eu}_{\text{N}*}$  versus  $\text{Ce}^{4+}/\text{Ce}^{3+}$  ratios of zircons from the granitoids in the Suyunhe large porphyry Mo deposit. (b) Mo tonnage of porphyry Mo deposits versus  $\text{Ce}^{4+}/\text{Ce}^{3+}$  ratios of zircons. (c) Mo tonnage of porphyry Cu deposits versus  $\text{Eu}_{\text{N}}/\text{Eu}_{\text{N}*}$  ratios of zircons. Data for small ( $0.6\text{--}<1.5 \text{ Mt Cu}$ ) porphyry Cu deposits (Borly and Baogutu) and intermediate-large ( $\geq 1.5 \text{ Mt Cu}$ ) porphyry Cu deposits (Bozhakol, Nurkazghan, Kounrad, Aktogai, Erdenet, Koksa, Tuwu–Yandong) are from Shen et al. (2015), and are representative of porphyry Cu deposits in the CAOB. Zircon trace element data of the Shapinggou porphyry Mo deposit (2.2 Mt; Zhang et al., 2014) and the Shuyaogou porphyry Mo deposit (0.15 Mt; Han et al., 2013) from the East Qinling–Dabie metallogenic belt, China, and the Dabaoshan porphyry Mo deposit (0.1–0.15 Mt; Li et al., 2012) from the Nanling metallogenic belt, China, are also shown. The Shapinggou and the Suyunhe deposits are representative of large porphyry Mo deposits, whereas the Shuyaogou and the Dabaoshan deposits are representative of small–intermediate porphyry Mo deposits in this study. Abbreviations: PMD, porphyry Mo deposit; PCD, porphyry Cu deposit. Symbols are as in Fig. 3.

Thus, we propose the following tectonic-magmatic model for the Suyunhe granites: at Late Carboniferous–Early Permian, the Suyunhe area came into a late subduction or *syn-collisional* (between Yili and Junggar terranes) stage; the juvenile lower crust, formed by deeply buried oceanic crust and oceanic island-arc series during complicated subduction-accretion processes (Chen and Arakawa, 2005), began to be thickened. The asthenosphere upwelling was introduced by a slab rollback, and the former then triggered partial melting of juvenile lower crust under the Suyunhe deposit. The partial melting of thickened juvenile lower crust (>40 km) left a garnet±amphibole residue and formed LSE with high Sr/Y, La/Yb and Mg#, whereas partial melting of shallower juvenile crust (~30 km) left a plagioclase residue and subsequently formed HSE with features of I-type granite. During ascending of magmas, HSE underwent strong plagioclase-dominated fractionation, whereas crystal fractionation in LSE was limited and weak.

#### 6.4. The relationship of the Suyunhe granites and Mo mineralization

##### 6.4.1. Magmatic oxidation state

Zircon is a remarkable mineral attributed to its ubiquitous occurrence, and trace element abundances in them have been shown to be sensitive to crystallization environments (Ballard et al., 2002; Belousova et al., 2002; Belousova, 2006; Trail et al., 2012; Zhao et al., 2016). Compared with other trivalent REEs, positive Ce anomalies can be observed in igneous zircon because that the identical charge and similar size of  $\text{Ce}^{4+}$  to Zr normally result in partition of  $\text{Ce}^{4+}$  into zircon in strong preference to  $\text{Ce}^{3+}$  (Ballard et al., 2002). Similar reason also renders that  $\text{Eu}^{3+}$  should be incorporated preferentially into zircon relative to  $\text{Eu}^{2+}$  and therefore results in Eu anomalies, although in most cases they are complicated because of the effects of a plagioclase residual in sources, and plagioclase crystallization during ascending of magmas, as well as assimilation of plagioclase-bearing rocks (Ballard et al., 2002; Han et al., 2013). In spite of this, large numbers of articles have recently confirmed that both  $\text{Ce}^{4+}/\text{Ce}^{3+}$  and  $\text{Eu}_{\text{N}}/\text{Eu}_{\text{N}*}$  ratios in zircon can be used as effective indicators of the magmatic oxidation state (e.g., Ballard et al., 2002; Han et al., 2013; Shen et al., 2015).

Zircons used for trace element analyses are all collected from ore-bearing HSE according to the above discussion. These samples show identical  $\text{Ce}^{4+}/\text{Ce}^{3+}$  and  $\text{Eu}_{\text{N}}/\text{Eu}_{\text{N}*}$  ratios, mainly ranging from 5 to 100 and 0.2 to 0.5 respectively. To evaluate the relationship between the magmatic oxidation state and productivity, we compare our results with I-type Kosciusko tonalite and S-type Berridale adamellite from the Lachlan fold belt (Belousova, 2006). Since there is no mineralization found in these two batholiths (Shen et al., 2015 and references therein), their respective zircon trace element compositions therefore could well represent those of barren granitoids. These barren granites show lower  $\text{Ce}^{4+}/\text{Ce}^{3+}$  and  $\text{Eu}_{\text{N}}/\text{Eu}_{\text{N}*}$  ratios than ore-bearing granites from the Suyunhe Mo deposit, ranging from 0.54 to 2.53 (average = 1.22; Shen et al., 2015) and 0.04 to 0.43 (average = 0.26) respectively. It indicates a link between magmatic oxidation state and mineralization.

Shen et al. (2015) confirmed that there was a clear relationship, at least in the CAOB, between the magmatic oxidation state and the sizes of porphyry Cu deposits. Based on the new data in this study and published data by (Li et al., 2012; Han et al., 2013; Shen et al., 2015), we here evaluate the relationship of magmatic oxidation state and the size of porphyry Mo deposits, as well as the relationship of magmatic oxidation state and the types of porphyry deposits. It is clearly shown in Fig. 12 that both  $\text{Ce}^{4+}/\text{Ce}^{3+}$  and  $\text{Eu}_{\text{N}}/\text{Eu}_{\text{N}*}$  of zircons from the Suyunhe are lower than those from small porphyry Cu deposit, let alone than those from intermediate-large

porphyry Cu deposits. Since all these deposits are from the CAOB, this might indicate that in the CAOB, parental magmas of large porphyry Mo deposits are less oxidized than those of porphyry Cu deposits. However, there are no published zircon trace element data of porphyry Mo deposits in the CAOB, which currently makes it impossible to evaluate the relationship between the magmatic oxidation state and the sizes of porphyry Mo deposits in the CAOB. Nevertheless, we still could compare  $\text{Ce}^{4+}/\text{Ce}^{3+}$  and  $\text{Eu}_{\text{N}}/\text{Eu}_{\text{N}*}$  ratios of zircons of the Suyunhe deposit with those of other porphyry Mo deposits from the East Qinling–Dabie and the Nanling metallogenic belts, China. The East Qinling–Dabie metallogenic belt boasts a resource of >6 Mt Mo metal and ranks as the most important Mo province in the world (Li and Pirajno, 2017). The Nanling metallogenic belt is the largest W–Sn mineralization belt in the world, with >60% and about 20% of the world's total W and Sn reserves, respectively; recent studies revealed that a few porphyry Mo and Cu deposits also occurred in this belt, of which the Dabaoshan porphyry Mo deposit is the largest one (Li et al., 2012). In Fig. 12, it is clearly displayed that small–intermediate porphyry Mo deposits show much higher  $\text{Ce}^{4+}/\text{Ce}^{3+}$  (mostly >200) and  $\text{Eu}_{\text{N}}/\text{Eu}_{\text{N}*}$  (mostly >0.5) than large porphyry Mo deposits (and some values are even higher than those of intermediate–large porphyry Cu deposits) (Fig. 12), which is just on the contrary to the circumstance found for porphyry Cu deposits (Shen et al., 2015). This might imply the different geochemical behaviors of Mo and Cu during the formation of porphyritic magmas, although the exact mechanism is beyond the scope of our knowledge. If our finding is correct, then the systematic decrease in zircon  $\text{Ce}^{4+}/\text{Ce}^{3+}$  and  $\text{Eu}_{\text{N}}/\text{Eu}_{\text{N}*}$  with the increasing sizes of porphyry Mo deposits means that unlike porphyry Cu deposits, too high oxygen fugacities do not boost the mineralization in porphyry Mo deposits, although much lower ones also are not conducive to Mo mineralization. We thus argue that an intermediate oxygen fugacity with  $\text{Ce}^{4+}/\text{Ce}^{3+}$  of about 5 to ~200 and  $\text{Eu}_{\text{N}}/\text{Eu}_{\text{N}*}$  of below 0.5 might be best benefit to formation of large porphyry Mo deposits. However, since all the selected porphyry Mo deposits are from China, more data from other places in the world are needed to test whether this finding is universally applicable.

#### 6.4.2. Adakite-like rocks: Productive or unproductive for porphyry Mo deposit?

Although lack of systematic trace element data of zircons from adakite-like LSE renders their  $\text{Ce}^{4+}/\text{Ce}^{3+}$  and  $\text{Eu}_{\text{N}}/\text{Eu}_{\text{N}*}$  unavailable, previous studies with regard to the adakites and adakite-like rocks have firmly illustrated their high oxygen fugacities relative to normal arc magmatic rocks (Castillo, 2006; Wang et al., 2006a; Hou et al., 2012, 2013; Sun et al., 2013, 2014; Zhang et al., 2013). Therefore, it can be deduced that LSE might have higher  $\text{Ce}^{4+}/\text{Ce}^{3+}$  (>100) and  $\text{Eu}_{\text{N}}/\text{Eu}_{\text{N}*}$  (>0.5) than HSE in the Suyunhe deposit. As noted above, we interpret that neither high nor low oxygen fugacities are favorable for porphyry Mo deposits (Fig. 12). If this interpretation is correct, then the high oxygen fugacities of LSE mean that they are unproductive. In fact, lot of evidence indeed indicates the LSE (mainly tonalite porphyry and granodiorite porphyry) of the Suyunhe Mo deposits are barren. (1) Hand specimen observations confirm that there is little Mo mineralization in LSE. (2) Although three stocks in the Suyunhe deposit are comparable in terms of volumes, all rocks from stock II are ore-bearing HSE, and stock I is composed of HSE and minor LSE, whereas stock III is composed of lower ratios of HSE and higher ratios of LSE compared to stock I; interesting, the majority of Mo mineralization (~62.9% molybdenum metal resources) occurred in stock II, stock I takes the second place, whereas only approximately 2.5% molybdenum

metal resources occurred in stock III (Zhong et al., 2015a). The negative correlation between LSE and Mo mineralization further indicates that adakites and adakite-like rocks are unproductive for porphyry Mo deposits, although they are very productive for porphyry Cu (–Au) deposits (Oyarzun et al., 2001; Reich et al., 2003; Wang et al., 2006a; Shafei et al., 2008; Li et al., 2011; Chiaradia et al., 2012; Hou et al., 2013; Shen et al., 2015). This might be not only applicable in the West Junggar, but also elsewhere in the world, in view that few porphyry Mo deposits are reported to be directly and/or indirectly related to adakitic rocks.

## 7. Conclusions

Two main types of granitoids (i.e., LSE and HSE) can be clearly distinguished on the basis of their silica and other major and trace elemental contents (e.g., MgO, Eu, Sr, Y, La, Yb). The contrasting distinctions of their chemical compositions emphasize differences of their sources and petrogenesis. Specifically, LSE show adakite-like features, i.e., high Mg<sup>#</sup> numbers (mostly >0.4), low Y and Yb concentrations, high Sr/Y and La/Yb ratios, and do not manifest clear crystal fractionation; in contrast, HSE display lower Mg<sup>#</sup> (<0.4) and Sr concentrations, higher Y and Yb concentrations, lower Sr/Y and La/Yb ratios, which are similar to those from normal arc rhyolite lavas. Besides, the extremely negative anomalies of Ba, Sr, P, Ti and Eu in HSE indicate a plagioclase-dominated fractionation.

HSE in the Suyunhe deposit likely formed by partial melting of juvenile lower crust at depths of less than ~33 km where a plagioclase residue existed. LSE were also derived from partial melting of juvenile lower crust, but their source was much deeper (>40 km) where melts were in equilibrium with a garnet-rich residue. The initial melting of (thickened) juvenile lower crust for LSE and HSE was both probably triggered by asthenosphere upwelling subsequent to a slab rollback event.

The  $\text{Ce}^{4+}/\text{Ce}^{3+}$  and  $\text{Eu}_{\text{N}}/\text{Eu}_{\text{N}*}$  ratios in zircons of HSE are much lower than ore-forming intrusions from porphyry Cu deposits in the CAOB, but noticeably higher than barren intrusions from the Lachlan fold belt and ore-bearing intrusions of small–intermediate porphyry Mo deposits from the East Qinling–Dabie and the Nanling metallogenic belts, China, indicating that neither too high nor too low oxygen fugacities are favorable for large porphyry Mo deposits. We argue that adakites and adakite-like rocks, at least in the West Junggar, are unproductive for porphyry Mo deposits.

## Acknowledgements

We thank Hongdi Pan, Wei Zhu, Ning Yu, and Yueheng Yang for provided access to drill core, underground workings and laboratories for sampling and experimental analyses. Financial support for this research was provided by the National Natural Science Foundation of China (grant Nos. U1303293, 41390442, 41272109), the IUGS–UNESCO (IGCP–592 project), the Key Deployment Project of the Chinese Academy of Sciences (grant No. KJZD-EW-TZ-G07), and the National 305 Project (grant No. 2011BAB06B01). The Editor-in-Chief, Professor Franco Pirajno and two anonymous reviewers are especially thanked for their helpful input to improve the manuscript.

## Appendix A.

See Supplementary Data in Appendix Table A1.

**Table A1**

Major (%) and trace element (ppm) analyses of granitoids in the Suyunhe large porphyry Mo deposit.

Sample No. Stock	S-12 I	S-15 I	S-16 I	S-17 I	S-19 I	S-20 I	S-21 I	S-22 I	Zk0809-255 I	ZK0003-261 I
Source	Yang et al. (2015)								Shen et al. (2013a)	
Rock	MGP?	MGP?	MGP?	MGP?	MGP?	MGP?	MGP?	MGP?	MGP	G
SiO <sub>2</sub>	74.22	74.22	72.8	73.79	69.75	68.48	74.08	74.11	76.66	78.75
Al <sub>2</sub> O <sub>3</sub>	14.08	13.76	13.91	13.81	15.31	15.19	14	13.68	12.97	11.97
TFeO	1.39	1.43	2.05	1.55	2.75	2.14	1.34	1.45	0.9	0.66
MgO	0.52	0.59	0.64	0.63	1.12	1.18	0.65	0.63	0.14	0.1
CaO	1.74	1.12	1.38	1.03	1.3	2.53	1.02	0.98	0.7	0.54
Na <sub>2</sub> O	3.87	3.75	3.73	3.6	3.72	3.81	4.07	3.89	3.56	3.15
K <sub>2</sub> O	3.01	3.44	3.55	3.73	3.21	2.99	3.09	3.2	5.17	5.11
MnO	0.04	0.05	0.06	0.05	0.03	0.04	0.05	0.06	0.02	0.01
TiO <sub>2</sub>	0.25	0.22	0.23	0.22	0.42	0.41	0.24	0.22	0.09	0.07
P <sub>2</sub> O <sub>5</sub>	0.08	0.07	0.08	0.08	0.14	0.14	0.08	0.09	0.02	0.01
LOI	1.07	0.94	1.32	1.03	1.77	3.32	1.04	2.11	0.04	0.05
Total	100.27	99.59	99.75	99.52	99.52	100.23	99.66	100.42	100.27	100.42
Ni	2.31	14.7	4.73	4.06	4.02	10.4	4.33	3.95	5.15	1.67
Ga	15.8	15.9	17.5	15.6	17.8	17.6	16.3	15.8	10.9	9.64
Rb	117	128	139	130	151	140	122	123	176	161
Sr	346	265	377	294	383	430	293	283	38.8	20.6
Ba	417	410	465	477	628	655	376	358	42.9	16.4
La	6.7	15.2	22.3	15.4	18.4	18	15.5	15.9	8.72	5.83
Ce	12.2	28.2	40.2	30.3	37.6	35.8	29.6	30.5	19.1	16.2
Pr	1.62	3.24	4.2	3.16	4.2	4.15	3.34	3.37	1.96	1.49
Nd	6.31	11.6	14.3	11.2	16.2	15.9	12	12.2	7.22	5.49
Sm	1.44	2.2	2.55	2.11	3.22	3.21	2.28	2.36	1.8	1.32
Eu	0.42	0.48	0.55	0.49	0.82	0.82	0.48	0.47	0.11	0.06
Gd	1.38	2	2.37	1.89	2.96	2.94	2.08	2.21	2.07	1.16
Tb	0.2	0.29	0.34	0.27	0.43	0.42	0.3	0.32	0.392	0.275
Dy	1.23	1.73	2.08	1.65	2.52	2.45	1.75	1.98	2.59	1.83
Ho	0.25	0.37	0.45	0.35	0.51	0.49	0.37	0.42	0.607	0.389
Er	0.78	1.15	1.37	1.05	1.5	1.44	1.13	1.31	2.14	1.58
Tm	0.13	0.19	0.23	0.17	0.24	0.23	0.19	0.22	0.466	0.305
Yb	0.94	1.41	1.65	1.24	1.6	1.52	1.37	1.62	3.11	2.3
Lu	0.16	0.23	0.27	0.2	0.25	0.24	0.22	0.26	0.606	0.439
Y	7.98	11.7	14	10.8	15.5	14.9	11.7	13.7	19.8	12.1
Pb	15	13.8	16	15.7	10.3	9.72	12.9	13.5	19.8	20.4
Th	8.3	9.9	12	9.37	6.3	6.02	10.4	10.6	18.9	22.2
U	4	3.57	2.89	2.64	4.06	6.57	3.53	3.22	12.6	22.6
Nb	4.99	6.06	6.99	5.33	6.96	6.57	6.78	7.05	13	25.4
Ta	0.65	0.7	0.9	0.65	0.61	0.66	0.85	0.97	2.95	3.36
Zr	91.9	91.4	100	94.6	128	122	85.1	87.1	67.1	74.9
Hf	2.82	2.87	3.16	2.88	3.57	3.37	2.75	2.85	4.05	5.08
A/CNK	1.10	1.15	1.11	1.17	1.28	1.08	1.18	1.17	1.02	1.02
Mg#	0.43	0.45	0.38	0.45	0.45	0.52	0.49	0.46	0.24	0.23
La/Yb	7.1	10.8	13.5	12.4	11.5	11.8	11.3	9.8	2.8	2.5
Sr/Y	43.4	22.6	26.9	27.2	24.7	28.9	25.0	20.7	2.0	1.7
Rb/Sr	0.3	0.5	0.4	0.4	0.4	0.3	0.4	0.4	4.5	7.8
δEu	0.91	0.70	0.68	0.75	0.81	0.82	0.67	0.63	0.17	0.15
Sample No. Stock	ZK0003-298 I	ZK0003-360 I	ZK0003-380 I	ZK0003-400 I	ZK0003-420 I	Zk5215-487 II	Zk6019-490 II	Zk6019-507 II	zk9235-447 III	zk9235-457 III
Source	Shen et al. (2013a)					Shen et al. (2017)				
Rock	G	G	G	G	G	G	GP	GP	GP	G
SiO <sub>2</sub>	78.37	77.74	75.55	76.44	76.73	72.95	76.55	76.39	76.07	75.87

Table A1 (continued)

Sample No.	ZK0003-298	ZK0003-360	ZK0003-380	ZK0003-400	ZK0003-420	Zk5215-487	Zk6019-490	Zk6019-507	zk9235-447	zk9235-457
Stock	I	I	I	I	I	II	II	II	III	III
Al <sub>2</sub> O <sub>3</sub>	12.35	12.58	12.94	12.41	12.49	13.34	12.52	13.05	12.93	13.04
TFeO	0.69	0.74	1.37	1.38	1.3	1.83	1.41	1.45	1.4	1.43
MgO	0.11	0.1	0.39	0.37	0.37	0.35	0.28	0.37	0.35	0.36
CaO	0.57	0.56	1.28	1.04	1.03	1.22	0.6	1.06	1.11	1.14
Na <sub>2</sub> O	3.5	3.83	3.68	3.45	3.35	3.54	3.01	3.76	3.64	3.75
K <sub>2</sub> O	4.78	4.51	4.01	4.2	4.39	4.68	5.61	4.2	4.22	4.1
MnO	0.02	0.04	0.05	0.04	0.04	0.05	0.04	0.05	0.05	0.05
TiO <sub>2</sub>	0.06	0.07	0.18	0.16	0.17	0.17	0.14	0.17	0.16	0.16
P <sub>2</sub> O <sub>5</sub>	0.01	0.01	0.04	0.04	0.04	0.03	0.03	0.04	0.03	0.04
LOI	0.05	0.05	0.62	0.88	0.56	1.95	0.04	0.04	0.34	0.38
Total	100.51	100.23	100.11	100.41	100.47	100.11	100.23	100.58	100.3	100.32
Ni	4.48	2.12	3.46	3.15	3.04	4.27	3.83	6.88	5.77	6.02
Ga	9.79	8.84	11.9	11.8	13.6	16	12.3	16.1	13.7	14.9
Rb	153	191	121	126	151	174	196	168	147	153
Sr	18.9	14.9	117	104	131	71	120	124	119	123
Ba	18.1	12.9	214	184	210	210	315	191	200	203
La	7.81	4.86	14.3	14.3	20.8	13.1	12.9	29.3	17.1	21.6
Ce	20.8	14.3	24.1	24.1	39.9	25.3	23.8	54.2	32.5	41.5
Pr	1.73	1.08	3.26	3.27	4.7	3.19	2.79	6.18	3.89	4.77
Nd	5.88	3.86	11.9	12.2	17.2	12.3	10.2	22.5	14.5	17.7
Sm	1.18	0.885	2.4	2.43	3.48	2.84	1.97	4.56	3.14	3.35
Eu	0.06	0.034	0.339	0.284	0.349	0.315	0.411	0.331	0.346	0.375
Gd	1.18	0.745	2.1	2.38	3.26	2.8	1.86	4.42	3.01	3.06
Tb	0.183	0.158	0.418	0.382	0.539	0.493	0.299	0.852	0.494	0.619
Dy	1.53	1.16	2.44	2.39	3.49	3.57	1.94	4.59	3.34	3.3
Ho	0.358	0.248	0.554	0.521	0.81	0.764	0.384	1.07	0.781	0.638
Er	1.25	1	1.66	1.5	2.31	2.48	1.08	3.18	2.29	2.08
Tm	0.294	0.227	0.377	0.312	0.497	0.49	0.234	0.704	0.432	0.38
Yb	2.2	1.53	2.46	2.37	3.31	3.56	1.91	4.56	3.04	2.89
Lu	0.366	0.249	0.39	0.371	0.506	0.625	0.252	0.768	0.476	0.564
Y	11.7	9.16	16.2	15.7	24.5	24.7	12.7	34.7	22.4	22.6
Pb	20.7	24.6	15.5	15.9	17.5	20	25.1	22.3	19.4	20.4
Th	20.8	16.9	13.2	11.2	20.4	17.9	13.2	20.1	17.5	20.5
U	16.8	8.02	4.84	5.18	8.7	6.5	5.91	9.85	8.77	8.46
Nb	12.7	10.9	9.02	10.1	11.5	13.3	7.44	14.5	12.6	9.68
Ta	1.69	1.6	1.27	1.38	1.6	2.07	0.984	3.01	1.56	1.45
Zr	83.8	72.8	72.2	72	96.5	85.1	58.7	85.5	68.9	129
Hf	4.92	4.07	3.14	2.88	4.06	3.77	2.35	4.65	2.6	5.09
A/CNK	1.03	1.03	1.02	1.02	1.03	1.02	1.03	1.03	1.03	1.03
Mg#	0.24	0.21	0.36	0.35	0.36	0.27	0.28	0.34	0.33	0.33
La/Yb	3.6	3.2	5.8	6.0	6.3	3.7	6.8	6.4	5.6	7.5
Sr/Y	1.6	1.6	7.2	6.6	5.3	2.9	9.4	3.6	5.3	5.4
Rb/Sr	8.1	12.8	1.0	1.2	1.2	2.5	1.6	1.4	1.2	1.2
δEu	0.16	0.13	0.46	0.36	0.32	0.34	0.66	0.23	0.34	0.36
Sample No.	zk9235-462	SYH1	SY3-5	SYP8-1	SYP8-2	SYP8-3	SYP8-4	11SYP9-2	11SYP9-3	ZK0003-214*
Stock	III	I	I	III	III	III	III	III	III	I

Shen et al. (2017)

S. Zhong et al. / Ore Geology Reviews 88 (2017) 116–139

(continued on next page)

**Table A1** (continued)

Sample No.	zk9235-462	SYH1	SY3-5	SYP8-1	SYP8-2	SYP8-3	SYP8-4	11SYP9-2	11SYP9-3	ZK0003-214*
Stock	III	I	I	III	III	III	III	III	III	I
Na <sub>2</sub> O	3.52	3.47	4.02	3.57	3.84	3.78	3.77	3.88	3.96	3.44
K <sub>2</sub> O	4.2	3.62	3.43	3.5	3.14	3.67	3.28	2.57	2.56	4.45
MnO	0.06	0.04	0.07	0.06	0.06	0.06	0.06	0.06	0.06	0.03
TiO <sub>2</sub>	0.18	0.25	0.45	0.34	0.37	0.33	0.36	0.43	0.44	0.13
P <sub>2</sub> O <sub>5</sub>	0.04	0.07	0.12	0.1	0.1	0.1	0.11	0.15	0.16	0.04
LOI	0.03	1.09	1.19	1.63	1.38	1.49	2.16	1.13	1.23	0.87
Total	100.18	100.64	100.34	100.17	100.39	100.54	100.55	99.95	99.97	99.72
Ni	15.9	3.46	3.84	4.99	4.42	4.57	4.43	6.71	7.7	1.21
Ga	13.9	12.1	15.9	15.7	14.9	15.6	13.2	16.1	17.3	16.6
Rb	147	135	136	101	84.9	95.2	85.3	59.1	62.1	153
Sr	121	324	258	408	428	359	361	496	505	72.7
Ba	218	482	752	858	806	729	716	617	627	155
La	20.9	9.85	29.1	23	19.8	23.9	17.8	19.3	20.5	13.1
Ce	39	18.5	50.3	46.2	35.7	40.3	41	34.5	38.2	27.9
Pr	4.5	2.57	6.48	5	4.04	4.91	4.14	4.17	4.74	3.32
Nd	16.4	9.54	24.7	19.1	15.6	19.1	16.1	17.4	17.4	12.1
Sm	3.17	1.87	4.71	3.48	3.09	3.59	3.14	3.05	3.14	2.68
Eu	0.382	0.427	1.07	0.741	0.747	0.82	0.764	0.81	0.97	0.22
Gd	2.84	1.61	3.78	2.98	2.51	2.94	3.16	2.64	2.99	2.35
Tb	0.524	0.199	0.607	0.432	0.393	0.436	0.384	0.44	0.48	0.49
Dy	3.05	1.59	3.82	2.67	2.94	2.95	2.51	2.39	2.22	3.2
Ho	0.62	0.296	0.787	0.574	0.564	0.572	0.496	0.39	0.51	0.68
Er	2.03	0.764	2.31	1.39	1.83	1.6	1.54	1.37	1.55	2.45
Tm	0.358	0.166	0.39	0.271	0.294	0.4	0.266	0.26	0.27	0.48
Yb	2.39	1.13	2.48	1.74	2.02	1.52	1.6	1.54	1.55	3.47
Lu	0.463	0.2	0.448	0.234	0.322	0.322	0.241	0.25	0.28	0.64
Y	20.2	9.57	21.5	15.7	17.5	17.4	14.8	13.7	14.3	23.8
Pb	19.2	12.8	14.6	15.2	11.4	14.2	11.8	9.68	9.86	22.3
Th	17.8	8.62	6.18	7.85	8.58	7.56	6.61	6.16	6.74	22.6
U	8.03	3.84	3.17	2.07	2.91	2.09	1.89	2.66	2.85	18.7
Nb	9.62	6.02	11.9	7.44	8.4	8.41	6.68	6.14	6.82	8.35
Ta	1.28	0.586	0.839	0.64	0.762	0.731	0.609	0.59	0.62	1.95
Zr	72.2	96.6	258	131	135	128	122	170	176	133
Hf	2.89	3.08	6.62	3.92	4.43	4.17	3.7	4.36	4.49	6.13
A/CNK	1.03	1.09	1.07	1.10	1.07	1.07	1.05	1.00	1.00	0.94
Mg#	0.34	0.50	0.32	0.41	0.41	0.40	0.41	0.43	0.44	0.29
La/Yb	8.7	8.7	11.7	13.2	9.8	15.7	11.1	12.5	13.2	3.8
Sr/Y	6.0	33.9	12.0	26.0	24.5	20.6	24.4	36.2	35.3	3.1
Rb/Sr	1.2	0.4	0.5	0.2	0.2	0.3	0.2	0.1	0.1	2.1
δEu	0.39	0.75	0.78	0.70	0.82	0.77	0.74	0.87	0.97	0.27
Sample No.	ZK0003-215*	ZK0003-221*	SYP13-2	SYP13-3	Syh1-1	Syh1-2	Syh1-3	Syh1-4	Syh1-5	Syh2-1
Stock	I	I	II	II	I	I	I	I	I	II
Source	<a href="#">Shen et al. (2017)</a>									
	<a href="#">Zhong et al. (2015a)</a>									
Rock	MGP	MGP	GP	GP	MGP	GDP	GDP	GDP	MGP	MGP
SiO <sub>2</sub>	75.97	75.7	80.08	78.7	77.34	73.22	73.84	70.97	76.8	72.78
Al <sub>2</sub> O <sub>3</sub>	11.7	12.42	11.21	12.17	11.57	13.1	12.96	14.63	12.25	13.91
TFeO	0.99	1.18	0.57	0.63	1.07	2.31	1.86	2.79	0.78	1.27
MgO	0.28	0.33	0.07	0.08	0.13	0.71	0.56	0.69	0.13	0.32
CaO	1.19	0.92	0.31	0.17	0.65	2.02	1.01	2.04	0.59	1.1
Na <sub>2</sub> O	3.49	4.04	3.15	3.52	3.07	3.76	3.62	3.1	3.47	4.05
K <sub>2</sub> O	4.89	4.47	4.48	4.65	4.83	3.16	4.03	4.53	4.83	4.91
MnO	0.04	0.04	0.02	0.03	0.02	0.06	0.05	0.1	0.02	0.04
TiO <sub>2</sub>	0.14	0.15	0.05	0.06	0.07	0.24	0.23	0.32	0.07	0.14
P <sub>2</sub> O <sub>5</sub>	0.04	0.04	0.01	0.02	0.02	0.08	0.07	0.11	0.01	0.03

**Table A1** (continued)

Sample No.	ZK0003-215*	ZK0003-221*	SYP13-2	SYP13-3	Syh1-1	Syh1-2	Syh1-3	Syh1-4	Syh1-5	Syh2-1
Stock	I	I	II	II	I	I	I	I	I	II
LOI	1	0.56	0.08	0.05	1.19	1.24	1.69	1.04	0.67	1.35
Total	99.73	99.85	100.03	100.08	99.96	99.9	99.92	100.32	99.62	99.9
Ni	1.25	1.64	3.263	1.85	7.5	9.6	7.7	6	3.8	6.6
Ga	16.1	17.3	13.6	14.6	10.5	14.1	15.2	18	14.3	16
Rb	166	160	87.3	103	158	115	144	142.5	161.5	174
Sr	82.2	117	23.3	31.4	38	251	142	264	48.9	83.7
Ba	182	303	64.8	102	52.5	420	406	491	54.9	211
La	13.6	14.8	3.68	12.5	9.7	14.2	11.5	24	7.2	16.6
Ce	29.1	31	8.02	23.5	18.7	23.6	22.7	50.3	15.9	29.5
Pr	3.32	3.53	1.26	3.2	2	2.9	2.4	5.7	1.7	3.7
Nd	12.2	12.3	4.95	12.8	7.4	10.3	9.3	21.4	6.1	12.9
Sm	2.77	2.52	1.52	3.43	1.3	1.8	1.8	4.8	1.6	2.6
Eu	0.22	0.33	0.134	0.19	0.11	0.48	0.37	0.83	0.14	0.31
Gd	2.46	2.4	1.54	3.3	1.27	1.52	1.64	4.48	1.57	2.07
Tb	0.54	0.53	0.37	0.617	0.3	0.3	0.3	0.7	0.3	0.4
Dy	3.37	3.3	2.79	4.04	1.9	1.3	1.9	4.6	2	2.5
Ho	0.77	0.75	0.579	0.811	0.4	0.3	0.4	1	0.5	0.5
Er	2.75	2.57	1.81	2.36	1.4	1	1.3	3.1	1.8	1.8
Tm	0.51	0.49	0.35	0.48	0.3	0.2	0.3	0.5	0.3	0.4
Yb	3.94	3.62	2.47	3.05	2.6	1.2	1.9	3.7	2.6	2.7
Lu	0.7	0.63	0.395	0.457	0.5	0.2	0.3	0.6	0.5	0.4
Y	25.8	24.9	17.3	25.2	14.7	8.5	13	30.6	18.2	17.5
Pb	22.1	19.4	15.3	17.6	18.3	11.9	15.9	15.3	18.2	17.1
Th	22	20.9	11.6	12.6	24.8	9.3	9.8	10.7	18	15.6
U	9.32	15.7	4.24	3.83	13.9	3.4	3.5	5.7	16.9	6.3
Nb	8.13	9.86	15.4	11.6	6.5	4.9	7.2	15.6	6.8	10.3
Ta	2.08	1.97	1.66	1.61	1.3	0.5	0.9	2	1.5	1.2
Zr	125	128	54.5	51.3	74.4	113	91.3	210	60	74.6
Hf	5.66	5.62	3.35	3.01	4	3.8	3.2	6.4	3.1	3.2
A/CNK	0.89	0.94	1.06	1.09	1.01	0.99	1.07	1.07	1.02	1.00
Mg#	0.36	0.36	0.20	0.20	0.19	0.38	0.37	0.33	0.25	0.33
La/Yb	3.5	4.1	1.5	4.1	3.7	11.8	6.1	6.5	2.8	6.1
Sr/Y	3.2	4.7	1.3	1.2	2.6	29.5	10.9	8.6	2.7	4.8
Rb/Sr	2.0	1.4	3.7	3.3	4.2	0.5	1.0	0.5	3.3	2.1
$\delta\text{Eu}$	0.26	0.41	0.27	0.17	0.26	0.89	0.66	0.55	0.27	0.41
Sample No.	Syh2-2	Syh2-3	Syh2-4	Syh2-5	Syh3-1	Syh3-2	Syh3-3	Syh3-4	Syh3-5	Syh3-6
Stock	II	II	II	II	III	III	III	III	III	III
Source	Zhong et al. (2015a)									
Rock	MGP	MGP	MGP	MGP	TP	TP	TP	GP	GDP	GP
SiO <sub>2</sub>	75.17	76.64	76.09	75.41	69.8	69.6	68.05	75.12	70.61	76.3
Al <sub>2</sub> O <sub>3</sub>	12.52	12.33	13.45	12.94	14.73	14.84	15.69	12.75	15.18	13.2
TFeO	1.65	1.29	1.08	1.34	2.95	3.11	3.5	1.45	1.83	1.45
MgO	0.42	0.27	0.22	0.29	0.96	1.02	1.32	0.36	0.47	0.34
CaO	0.85	0.62	1	1.03	1.97	2.06	3.71	1.1	1.39	1.13
Na <sub>2</sub> O	4.07	4.79	4.26	3.79	3.78	3.88	4.03	3.64	4.53	4.08
K <sub>2</sub> O	4.07	3.32	3.91	4.31	3.22	3.42	2.06	4.18	4.51	3.77
MnO	0.06	0.04	0.03	0.05	0.06	0.06	0.06	0.05	0.06	0.05
TiO <sub>2</sub>	0.18	0.14	0.12	0.14	0.37	0.38	0.46	0.17	0.19	0.16
P <sub>2</sub> O <sub>5</sub>	0.04	0.02	0.02	0.03	0.11	0.12	0.16	0.04	0.05	0.04
LOI	0.9	0.62	0.36	0.37	1.99	1.42	0.94	0.28	0.38	0.28
Total	99.93	100.08	100.54	99.7	99.94	99.91	99.98	99.14	99.2	100.8
Ni	8.7	6.5	3.9	5.7	7	7.8	8.9	5.4	5.1	5.7
Ga	13.5	14.3	14.9	14.9	17.2	16.7	16.9	14.5	18.4	14.8

(continued on next page)

**Table A1** (continued)

Sample No. Stock	Syh2-2 II	Syh2-3 II	Syh2-4 II	Syh2-5 II	Syh3-1 III	Syh3-2 III	Syh3-3 III	Syh3-4 III	Syh3-5 III	Syh3-6 III
Rb	143	177	154.5	164	86.3	95.9	51.7	154	175	149.5
Sr	106	54.4	105	105.5	325	344	574	118	141	117.5
Ba	228	107.5	144	176.5	808	899	715	212	228	196
La	18.7	12.7	12.3	14.3	18.3	18.8	22.2	17.3	19.5	21.4
Ce	36.3	28.8	26.7	30.6	33.8	35.7	39.2	36.9	41.4	43.8
Pr	4.2	3.1	3	3.4	3.9	4.2	4.5	4.1	4.6	4.7
Nd	15	11.5	11.4	12.8	15.4	16.3	17.7	14.6	16	16.3
Sm	3	2.7	2.9	3	3.3	3.5	3.1	3.2	3.5	3.3
Eu	0.35	0.19	0.25	0.31	0.82	0.85	0.88	0.31	0.39	0.36
Gd	2.93	2.53	2.73	2.77	2.96	2.99	2.62	2.64	3.15	2.82
Tb	0.5	0.4	0.5	0.5	0.5	0.5	0.5	0.5	0.5	0.4
Dy	3.1	3	3.5	3.2	2.8	2.9	2.3	3.1	3.5	3
Ho	0.7	0.6	0.7	0.7	0.6	0.6	0.4	0.7	0.7	0.7
Er	2.3	2.1	2.6	2.5	1.7	1.6	1.2	2.3	2.4	2.3
Tm	0.4	0.4	0.5	0.4	0.3	0.3	0.2	0.4	0.4	0.4
Yb	3.3	3	3.8	3	2	1.9	1.3	3.1	3.1	3
Lu	0.5	0.5	0.6	0.5	0.3	0.3	0.2	0.5	0.6	0.5
Y	21.4	19.3	25.3	23.6	16.5	16.3	11.9	22.7	24.6	22.5
Pb	18.2	21.3	21.1	21.7	13	13.1	10.6	21	23.1	20.9
Th	13.7	20.1	19.4	17	7.4	6.6	5	18.9	22.8	20.1
U	4.8	16.7	13.4	10.2	6.3	2.4	1.3	10	10.5	9.3
Nb	12	30.2	15.6	11	6.5	6.6	5.5	11.8	13.7	9.2
Ta	1.3	1.8	1.8	1.5	0.5	0.6	0.4	1.4	1.5	1.5
Zr	109	70	75	82	177	153	124	93	93	84
Hf	4.3	3.1	3.9	3.8	4.9	4.4	3.8	4.1	3.8	3.8
A/CNK	0.99	0.98	1.03	1.01	1.11	1.07	1.01	1.02	1.02	1.03
Mg#	0.34	0.29	0.29	0.30	0.39	0.39	0.43	0.33	0.34	0.32
La/Yb	5.7	4.2	3.2	4.8	9.2	9.9	17.1	5.6	6.3	7.1
Sr/Y	5.0	2.8	4.2	4.5	19.7	21.1	48.2	5.2	5.7	5.2
Rb/Sr	1.3	3.3	1.5	1.6	0.3	0.3	0.1	1.3	1.2	1.3
$\delta\text{Eu}$	0.36	0.22	0.27	0.33	0.80	0.80	0.94	0.33	0.36	0.36

## References

- Atherton, M.P., Petford, N., 1993. Generation of sodium-rich magmas from newly underplated basaltic crust. *Nature* 362, 144–146.
- Ballard, J.R., Palin, M.J., Campbell, I.H., 2002. Relative oxidation states of magmas inferred from Ce(IV)/Ce(III) in zircon: application to porphyry copper deposits of northern Chile. *Contrib. Mineral. Petro.* 144, 347–364.
- Belousova, E.A., 2006. Zircon crystal morphology, trace element signatures and hafnium isotope composition as a tool for petrogenetic modelling: examples from eastern Australian granitoids. *J. Petrol.* 47, 329–353.
- Belousova, E., Griffin, W., O'Reilly, S.Y., Fisher, N., 2002. Igneous zircon: trace element composition as an indicator of source rock type. *Contrib. Mineral. Petro.* 143, 602–622.
- Bourdon, E., Eissen, J.P., Monzier, M., Robin, C., Martin, H., Cotton, J., Hall, M.L., 2002. Adakite-like lavas from Antisana Volcano (Ecuador): evidence for slab melt metasomatism beneath Andean Northern Volcanic Zone. *J. Petrol.* 43, 199–217.
- Cao, M.J., Qin, K.Z., Li, G.M., Yang, Y.H., Evans, N.J., Zhang, R., Jin, L.Y., 2014. Magmatic process recorded in plagioclase at the Baogutu reduced porphyry Cu deposit, western Junggar, NW-China. *J. Asian Earth Sci.* 82, 136–150.
- Cao, C., Shen, P., Li, C.H., Zheng, G.P., 2016. Fluid inclusions and C-H-O-S isotope systematics of early Permian porphyry Mo mineralization of the West Junggar region, NW China: the Suyunhe example. *Int. Geol. Rev.* <http://dx.doi.org/10.1080/00206814.2016.1259082>.
- Castillo, P.R., 2006. An overview of adakite petrogenesis. *Chin. Sci. Bull.* 51, 257–268.
- Castillo, P.R., 2012. Adakite petrogenesis. *Lithos* 134–135, 304–316.
- Castillo, R.P., Janney, E.P., Solidum, U.R., 1999. Petrology and geochemistry of Camiguin Island, southern Philippines: insights to the source of adakites and other lavas in a complex arc setting. *Contrib. Mineral. Petro.* 134, 33–51.
- Chappell, B., White, A., 1992. I- and S-type granites in the Lachlan Fold Belt. *Trans. R. Soc. Edinb. Earth Sci.* 83, 1–26.
- Chen, B., Arakawa, Y., 2005. Elemental and Nd-Sr isotopic geochemistry of granitoids from the West Junggar foldbelt (NW China), with implications for Phanerozoic continental growth. *Geochim. Cosmochim. Acta* 69, 1307–1320.
- Chen, S., Guo, S.J., 2010. Time constraints, tectonic setting of Dalabute ophiolitic complex and its significance for Late Paleozoic tectonic evolution in West Junggar. *Acta Petrol. Sin.* 26, 2336–2344 (in Chinese with English abstract).
- Chen, B., Jahn, B.M., 2004. Genesis of post-collisional granitoids and basement nature of the Junggar Terrane, NW China: Nd-Sr isotope and trace element evidence. *J. Asian Earth Sci.* 23, 691–703.
- Chen, F., Satir, M., Ji, J., Zhong, D., 2002. Nd-Sr-Pb isotopes of Tengchong Cenozoic volcanic rocks from western Yunnan, China: evidence for an enriched-mantle source. *J. Asian Earth Sci.* 21, 39–45.
- Chen, J.F., Han, B.F., Ji, J.Q., Zhang, L., Xu, Z., He, G.Q., Wang, T., 2010. Zircon U-Pb ages and tectonic implications of Paleozoic plutons in northern West Junggar, North Xinjiang, China. *Lithos* 115, 137–152.
- Chiaradia, M., Ulianov, A., Kouzmanov, K., Beate, B., 2012. Why large porphyry Cu deposits like high Sr/Y magmas? *Sci. Rep.* 2, 1–7.
- Defant, M.J., Drummond, M.S., 1993. Mount St. Helens: potential example of the partial melting of the subducted lithosphere in a volcanic arc. *Geology* 21, 547–550.
- Dolgopolova, A., Seltmann, R., Armstrong, R., Belousova, E., Pankhurst, R.J., Kavalieris, I., 2013. Sr-Nd-Pb-Hf isotope systematics of the Hugo Dummett Cu-Au porphyry deposit (Oyu Tolgoi, Mongolia). *Lithos* 164, 47–64.
- Geng, H.Y., Sun, M., Yuan, C., Xiao, W.J., Xian, W.S., Zhao, G.C., Zhang, L.F., Wong, K., Wu, F.Y., 2009. Geochemical, Sr-Nd and zircon U-Pb-Hf isotopic studies of Late Carboniferous magmatism in the West Junggar, Xinjiang: implications for ridge subduction? *Chem. Geol.* 266, 364–389.
- Geng, H.Y., Sun, M., Yuan, C., Zhao, G.C., Xiao, W.J., 2011. Geochemical and geochronological study of early Carboniferous volcanic rocks from the West Junggar: petrogenesis and tectonic implications. *J. Asian Earth Sci.* 42, 854–866.
- Green, T.H., 1994. Experimental studies of trace-element partitioning applicable to igneous petrogenesis — Sedona 16 years later. *Chem. Geol.*, 1–36
- Han, Y.G., Zhang, S.H., Pirajno, F., Zhou, X.W., Zhao, G.C., Qü, W.J., Liu, S.H., Zhang, J.M., Liang, H.B., Yang, K., 2013. U-Pb and Re-Os isotopic systematics and zircon Ce<sup>4+</sup>/Ce<sup>3+</sup> ratios in the Shiyagou Mo deposit in eastern Qinling, central China: insights into the oxidation state of granitoids and Mo (Au) mineralization. *Ore Geol. Rev.* 55, 29–47.
- Hou, Z.Q., Zheng, Y.C., Yang, Z.M., Rui, Z.Y., Zhao, Z.D., Jiang, S.H., Qu, X.M., Sun, Q.Z., 2012. Contribution of mantle components within juvenile lower-crust to collisional zone porphyry Cu systems in Tibet. *Miner. Deposita* 48, 173–192.
- Hou, Z.Q., Pan, X.F., Li, Q.Y., Yang, Z.M., Song, Y.C., 2013. The giant Dexing porphyry Cu-Mo-Au deposit in east China: product of melting of juvenile lower crust in an intracontinental setting. *Miner. Deposita* 48, 1019–1045.
- Huang, X.L., Xu, Y.G., Lan, J.B., Yang, Q.J., Luo, Z.Y., 2009. Neoproterozoic adakitic rocks from Mopanshan in the western Yangtze Craton: partial melts of a thickened lower crust. *Lithos* 112, 367–381.
- Jin, H.J., Li, Y.C., Li, J.Y., 1987. Discovery and study of Carboniferous deep-water sediments in the northwest of Junggar Basin, Xinjiang. *Acta Sedime. Sin.* 125–134 (in Chinese with English abstract)
- Kay, R.W., Mahlburg, K.S., 1993. Delamination and delamination magmatism. *Tectonophysics* 219, 177–189.
- Kröner, A., Kovach, V., Belousova, E., Hegner, E., Armstrong, R., Dolgopolova, A., Seltmann, R., Alexeiev, D.V., Hoffmann, J.E., Wong, J., 2014. Reassessment of continental growth during the accretionary history of the Central Asian Orogenic Belt. *Gondwana Res.* 25, 103–125.
- Li, N., Pirajno, F., 2017. Early Mesozoic Mo mineralization in the Qinling Orogen: an overview. *81. Ore Geol. Rev.* 81 (Part 2), 431–450.
- Li, X.Z., Han, B.F., Ji, J.Q., Li, Z.H., Liu, Z.Q., Yang, B., 2004. Geology, geochemistry and K-Ar ages of Kalamay basic-intermediate dyke swarm from Xinjiang, China. *Geochemica* 33, 574–584 (in Chinese with English abstract).
- Li, J.W., Zhao, X.F., Zhou, M.F., Ma, C.Q., de Souza, Z.S., Vasconcelos, P., 2009. Late Mesozoic magmatism from the Daye region, eastern China: U-Pb ages, petrogenesis, and geodynamic implications. *Contrib. Mineral. Petro.* 157, 383–409.
- Li, J.X., Qin, K.Z., Li, G.M., Xiao, B., Chen, L., Zhao, J.X., 2011. Post-collisional ore-bearing adakitic porphyries from Gangdese porphyry copper belt, southern Tibet: melting of thickened juvenile arc lower crust. *Lithos* 126, 265–277.
- Li, C.Y., Zhang, H., Wang, F.Y., Liu, J.Q., Sun, Y.L., Hao, X.L., Li, Y.L., Sun, W.D., 2012. The formation of the Dabaoshan porphyry molybdenum deposit induced by slab rollback. *Lithos* 150, 101–110.
- Li, G.M., Cao, M.J., Qin, K.Z., Evans, N.J., McInnes, B.I.A., Liu, Y.S., 2014. Thermal-tectonic history of the Baogutu porphyry Cu deposit, West Junggar as constrained from zircon U-Pb, biotite Ar/Ar and zircon/apatite (U-Th)/He dating. *J. Asian Earth Sci.* 79, 741–758.
- Li, C.H., Shen, P., Pan, H.D., et al., 2016. Carboniferous porphyry Cu(-Au) mineralization of the West Junggar Region, NW China: the Shiwu example. *Int. Geol. Rev.* 10.1080/00206814.2016.1253037.
- Liu, X.J., Xu, J.F., Wang, S.Q., Hou, Y.Q., Bai, Z.H., Lei, M., 2009. Geochemistry and dating of E-MORB type mafic rocks from Dalabute ophiolite in West Junggar, Xinjiang and geological implications. *Acta Petrol. Sin.* 25, 1373–1389 (in Chinese with English abstract).
- Long, X.P., Wilde, S.A., Wang, Q., Yuan, C., Wang, X.C., Li, J., Jiang, Z., Dan, W., 2015. Partial melting of thickened continental crust in central Tibet: evidence from geochemistry and geochronology of Eocene adakitic rhyolites in the northern Qiangtang Terrane. *Earth Planet. Sci. Lett.* 414, 30–44.
- Macpherson, C.G., Dreher, S.T., Thirlwall, M.F., 2006. Adakites without slab melting: high pressure differentiation of island arc magma, Mindanao, the Philippines. *Earth Planet. Sci. Lett.* 243, 581–593.
- Martin, H., Smithies, R.H., Rapp, R., Moyen, J.F., Champion, D., 2005. An overview of adakite, tonalite-trondjemite-granodiorite (TTG), and sanukitoid: relationships and some implications for crustal evolution. *Lithos* 79, 1–24.
- Oyarzun, R., Márquez, A., Lillo, J., López, I., Rivera, S., 2001. Giant versus small porphyry copper deposits of Cenozoic age in northern Chile: adakitic versus normal calc-alkaline magmatism. *Miner. Deposita* 36, 794–798.
- Pirajno, F., Mao, J.W., Zhang, Z.C., Zhang, Z.H., Chai, F.M., 2008. The association of mafic-ultramafic intrusions and A-type magmatism in the Tian Shan and Altay orogens, NW China: implications for geodynamic evolution and potential for the discovery of new ore deposits. *J. Asian Earth Sci.* 32, 165–183.
- Pirajno, F., Seltmann, R., Yang, Y., 2011. A review of mineral systems and associated tectonic settings of northern Xinjiang, NW China. *Geosci. Front.* 2, 157–185.
- Prouteau, G., Scaillet, B., Pichavant, M., Maury, R., 2001. Evidence for mantle metasomatism by hydrous silicic melts derived from subducted oceanic crust. *Nature* 410, 197–200.
- Qin, J.F., Lai, S.C., Grapes, R., Diwu, C.R., Ju, Y.J., Li, Y.F., 2010. Origin of Late Triassic high-Mg adakitic granitoid rocks from the Dongjiangkou area, Qinling orogen, central China: implications for subduction of continental crust. *Lithos* 120, 347–367.
- Rapp, R.P., Watson, E.B., 1995. Dehydration melting of metabasalt at 8–32 kbar: implications for continental growth and crust-mantle recycling. *J. Petrol.* 36, 891–931.
- Rapp, R.P., Shimizu, N., Norman, M.D., Applegate, G.S., 1999. Reaction between slab-derived melts and peridotite in the mantle wedge: experimental constraints at 3.8 GPa. *Chem. Geol.* 160, 335–356.
- Reich, M., Parada, M.A., Palacios, C., Dietrich, A., Schultz, F., Lehmann, B., 2003. Adakite-like signature of Late Miocene intrusions at the Los Pelambres giant porphyry copper deposit in the Andes of central Chile: metallogenetic implications. *Miner. Deposita* 38, 876–885.
- Richards, J.P., Kerrich, R., 2007. Special paper: adakite-like rocks: their diverse origins and questionable role in metallogenesis. *Econ. Geol.* 102, 537–576.
- Richards, J.P., Spell, T., Rameh, E., Razique, A., Fletcher, T., 2012. High Sr/Y magmas reflect arc maturity, high magmatic water content, and porphyry Cu±Mo±Au potential: examples from the Tethyan arcs of Central and Eastern Iran and Western Pakistan. *Econ. Geol.* 107, 295–332.
- Safonova, I., Seltmann, R., Kroner, A., Gladkochub, D., Schulmann, K., Xiao, W.J., Kim, J., Komiya, T., Sun, M., 2011. A new concept of continental construction in the Central Asian Orogenic Belt. *Episodes* 34, 186–196.
- Sajona, F.G., Maury, R.C., Bellon, H., Cotton, J., Defant, M.J., Pubellier, M., 1993. Initiation of subduction and the generation of slab melts in western and eastern Mindanao, Philippines. *Geology* 21, 1007–1010.
- Seltmann, R., Konopelko, D., Biske, G., Divaev, F., Sergeev, S., 2011. Hercynian post-collisional magmatism in the context of Paleozoic magmatic evolution of the Tien Shan orogenic belt. *J. Asian Earth Sci.* 42, 821–838.
- Shafei, B., Haschke, M., Shahabpour, J., 2008. Recycling of orogenic arc crust triggers porphyry Cu mineralization in Kerman Cenozoic arc rocks, southeastern Iran. *Miner. Deposita* 44, 265–283.
- Shen, Y., Jin, C., 1993. The Relationships of Magma Activity and Gold Mineralization in West Junggar. Science Press, Beijing, pp. 137–135 (in Chinese).
- Shen, P., Pan, H.D., 2013. Country-rock contamination of magmas associated with the Baogutu porphyry Cu deposit, Xinjiang, China. *Lithos* 177, 451–469.

- Shen, P., Pan, H.D., 2015. Methane origin and oxygen-fugacity evolution of the Baogutu reduced porphyry Cu deposit in the West Junggar terrain. *China Miner. Deposita* 8, 967–986.
- Shen, P., Shen, Y.C., Pan, H.D., Wang, J.B., Zhang, R., Zhang, Y., 2010. Baogutu porphyry Cu-Mo-Au Deposit, West Junggar, Northwest China: petrology, alteration, and mineralization. *Econ. Geol.* 105, 947–970.
- Shen, P., Shen, Y.C., Pan, H.D., Li, X.H., Dong, L.H., Wang, J.B., Zhu, H.P., Dai, H.W., Guan, W.N., 2012. Geochronology and isotope geochemistry of the Baogutu porphyry copper deposit in the West Junggar region, Xinjiang, China. *J. Asian Earth Sci.* 49, 99–115.
- Shen, P., Pan, H.D., Xiao, W.J., Chen, X.H., Eleonorad, S., Shen, Y.C., 2013a. Two geodynamic-metallogenetic events in the Balkhash (Kazakhstan) and the West Junggar (China): carboniferous porphyry Cu and Permian greisen W-Mo mineralization. *Int. Geol. Rev.* 55, 1660–1687.
- Shen, P., Xiao, W.J., Pan, H.D., Dong, L.H., Li, C., 2013b. Petrogenesis and tectonic settings of the Late Carboniferous Jiamantieliek and Baogutu ore-bearing porphyry intrusions in the southern West Junggar, NW China. *J. Asian Earth Sci.* 75, 158–173.
- Shen, P., Hattori, K., Pan, H.D., Jackson, S., Seitmuratova, E., 2015. Oxidation condition and metal fertility of granitic magmas: zircon trace-element data from porphyry Cu Deposits in the Central Asian Orogenic Belt. *Econ. Geol.* 110, 1861–1878.
- Shen, P., Pan, H., Cao, C., Zhong, S.H., Li, C.H., 2017. The formation of the Suyunhe large porphyry Mo deposit in the West Junggar Terrain, NW China: zircon U-Pb Age, geochemistry and Sr-Nd-Hf Isotopic results. *Ore Geol. Rev.* 81, 808–828.
- Song, C.H., Wang, J.R., Huang, H.F., 1996. Study of deep-water sediments of Tailegula formation on the north of Baijiantan, West of Junggar Basin. *J. Lanzhou Univ. (Nat. Sci.)* 32, 136–141 (in Chinese with English abstract).
- Stern, R.C., Kilian, R., 1996. Role of the subducted slab, mantle wedge and continental crust in the generation of adakites from the Andean Austral Volcanic Zone. *Contrib. Mineral. Petrol.* 123, 263–281.
- Streck, M.J., Leeman, W.P., Chesley, J., 2007. High-magnesian andesite from Mount Shasta: a product of magma mixing and contamination, not a primitive mantle melt. *Geology* 35, 351.
- Sun, S.S., McDonough, W.F., 1989. Chemical and isotopic systematics of oceanic basalts: implications for mantle composition and processes. *Geol. Soc. Spec. Publ.* 42, 313–345.
- Sun, W.D., Ling, M.X., Chung, S.L., Ding, X., Yang, X.Y., Liang, H.Y., Fan, W.M., Goldfarb, R., Yin, Q.Z., 2012. Geochemical constraints on adakites of different origins and copper mineralization. *J. Geol.* 120, 105–120.
- Sun, W.D., Liang, H.Y., Ling, M.X., Zhan, M.Z., Ding, X., Zhang, H., Yang, X.Y., Li, Y.L., Ireland, T.R., Wei, Q.R., 2013. The link between reduced porphyry copper deposits and oxidized magmas. *Geochim. Cosmochim. Acta* 103, 263–275.
- Sun, W.D., Huang, R.F., Liang, H.Y., Ling, M.X., Li, C.Y., Ding, X., Zhang, H., Yang, X.Y., Ireland, T., Fan, W.M., 2014. Magnetite-hematite, oxygen fugacity, adakite and porphyry copper deposits: reply to Richards. *Geochim. Cosmochim. Acta* 126, 646–649.
- Tang, G.J., Wang, Q., Wyman, D.A., Li, Z.X., Zhao, Z.H., Jia, X.H., Jiang, Z.Q., 2010. Ridge subduction and crustal growth in the Central Asian Orogenic Belt: evidence from Late Carboniferous adakites and high-Mg diorites in the western Junggar region, northern Xinjiang (west China). *Chem. Geol.* 277, 281–300.
- Tang, G.J., Wang, Q., Wyman, D.A., Li, Z.X., Xu, Y.G., Zhao, Z.H., 2012a. Recycling oceanic crust for continental crustal growth: Sr-Nd-Hf isotope evidence from granitoids in the western Junggar region, NW China. *Lithos* 128, 73–83.
- Tang, G.J., Wang, Q., Wyman, D.A., Li, Z.X., Zhao, Z.H., Yang, Y.H., 2012b. Late Carboniferous high  $\epsilon$  Nd (t)- $\epsilon$  Hf (t) granitoids, enclaves and dikes in western Junggar, NW China: ridge-subduction-related magmatism and crustal growth. *Lithos* 140, 86–102.
- Tang, G.J., Wyman, D.A., Wang, Q., Li, J., Li, Z.X., Zhao, Z.H., Sun, W.D., 2012c. Asthenosphere-lithosphere interaction triggered by a slab window during ridge subduction: trace element and Sr-Nd-Hf-Os isotopic evidence from Late Carboniferous tholeiites in the western Junggar area (NW China). *Earth Planet. Sci. Lett.* 329–330, 84–96.
- Trail, D., Bruce Watson, E., Tailby, N.D., 2012. Ce and Eu anomalies in zircon as proxies for the oxidation state of magmas. *Geochim. Cosmochim. Acta* 97, 70–87.
- Wang, R., Zhu, Y., 2007. Geology of the Baobei gold deposit in Western Juggar and zircon SHRIMP age of its wall-rocks, Western Junggar (Xinjiang, NW China). *Geol. J. China Univ.* 13, 590–602 (in Chinese with English abstract).
- Wang, Q., McDermott, F., Xu, J.F., Bellon, H., Zhu, Y.T., 2005. Cenozoic K-rich adakitic volcanic rocks in the Hohxil area, northern Tibet: lower-crustal melting in an intracontinental setting. *Geology* 33, 465–468.
- Wang, Q., Wyman, D.A., Xu, J.F., Zhao, Z.H., Jian, P., Xiong, X.L., Bao, Z.W., Li, C.F., Bai, Z.H., 2006a. Petrogenesis of Cretaceous adakitic and shoshonitic igneous rocks in the Luzong area, Anhui Province (eastern China): implications for geodynamics and Cu-Au mineralization. *Lithos* 89, 424–446.
- Wang, Q., Xu, J.F., Jian, P., Bao, Z.W., Zhao, Z.H., Li, C.F., Xiong, X.L., Ma, J.L., 2006b. Petrogenesis of adakitic porphyries in an extensional tectonic setting, Dexing, South China: implications for the genesis of porphyry copper mineralization. *J. Petrol.* 47, 119–144.
- Wang, Q., Wyman, D.A., Xu, J., Dong, Y., Vasconcelos, P.M., Pearson, N., Wan, Y., Dong, H., Li, C., Yu, Y., Zhu, T., Feng, X., Zhang, Q., Zi, F., Chu, Z., 2008. Eocene melting of subducting continental crust and early uplift of central Tibet: evidence from central-western Qiangtang high-K calc-alkaline andesites, dacites and rhyolites. *Earth Planet. Sci. Lett.* 272, 158–171.
- Wen, Z.G., Zhao, W.P., Liu, T.F., Liu, S.B., 2016. Formation age and geotectonic significance of Baerluke ophiolite in West Junggar, Xinjiang. *Geol. Bull. China* 35, 1401–1410 (in Chinese with English abstract).
- Weng, K., Xu, X.Y., Ma, Z.P., Chen, Y.L., Sun, J.M., Zhang, X., 2016. The geochemistry and chronology characteristics and the geological significance of ultramafic rock in Mayile ophiolite, West Junggar, Xinjiang. *Acta Petrol. Sin.* 32, 1420–1436 (in Chinese with English abstract).
- Windley, B.F., Alexeev, D., Xiao, W.J., Kröner, A., Badarch, G., 2007. Tectonic models for accretion of the Central Asian Orogenic Belt. *J. Geol. Soc.* 164, 31–47.
- Xiao, W.J., Santosh, M., 2014. The western Central Asian Orogenic Belt: a window to accretionary orogenesis and continental growth. *Gondwana Res.* 25, 1429–1444.
- Xiao, W.J., Kröner, A., Windley, B., 2009a. Geodynamic evolution of Central Asia in the Paleozoic and Mesozoic. *Int. J. Earth Sci.* 98, 1185–1188.
- Xiao, W.J., Windley, B.F., Yong, Y., Yan, Z., Yuan, C., Liu, C., Li, J., 2009b. Early Paleozoic to Devonian multiple-accretionary model for the Qilian Shan, NW China. *J. Asian Earth Sci.* 35, 323–333.
- Xiao, W.J., Windley, B.F., Huang, B.C., Han, C.M., Yuan, C., Chen, H.L., Sun, M., Sun, S., Li, J.L., 2009c. End-Permian to mid-Triassic termination of the accretionary processes of the southern Altaids: implications for the geodynamic evolution, Phanerozoic continental growth, and metallogeny of Central Asia. *Int. J. Earth Sci.* 98, 1189–1217.
- Xie, G., Mao, J., Zhao, H., Duan, C., Yao, L., 2011. Zircon U-Pb and phlogopite 40Ar-39Ar age of the Chengchao and Jinshandian skarn Fe deposits, southeast Hubei Province, Middle-Lower Yangtze River Valley metallogenic belt, China. *Miner. Deposita* 47, 633–652.
- Xiong, X.L., Adam, J., Green, T.H., 2005. Rutile stability and rutile/melt HFSE partitioning during partial melting of hydrous basalt: implications for TTG genesis. *Chem. Geol.* 218, 339–359.
- Xu, J.F., Shinjo, R., Defant, M.J., Wang, Q., Rapp, R.P., 2002. Origin of Mesozoic adakitic intrusive rocks in the Ningzhen area of east China: partial melting of delaminated lower continental crust? *Geology* 30, 1111–1114.
- Xu, X., He, G.Q., Li, H., Ding, T.F., Liu, X.Y., Mei, S.W., 2006. Basic characteristics of the Karamay ophiolitic mélange, Xinjiang, and its zircon SHRIMP dating. *Geol. China* 33, 470–475 (in Chinese with English abstract).
- Xu, Z., Han, B.F., Ren, R., Zhou, Y.Z., Zhang, L., Chen, J.F., Su, L., Li, X.H., Liu, D.Y., 2012. Ultramafic-mafic mélange, island arc and post-collisional intrusions in the Mayile Mountain, West Junggar, China: implications for Paleozoic intra-oceanic subduction-accretion process. *Lithos* 132–133, 141–161.
- Xu, Z., Han, B.F., Ren, R., Zhou, Y.Z., Su, L., 2013. Palaeozoic multiphase magmatism at Barleik Mountain, southern West Junggar, Northwest China: implications for tectonic evolution of the West Junggar. *Int. Geol. Rev.* 55, 633–656.
- Yan, Y.H., Shen, P., Pan, H.D., Wang, J.N., Zhong, S.H., Liu, X.G., 2014. Fluid inclusion and geochronology study of the Hongyuan Mo deposit and Tuketuke Mo(Cu) deposit, Western Junggar, Xinjiang. *Chin. J. Geol.* 49, 287–304 (in Chinese with English abstract).
- Yang, G.X., Li, Y.J., Gu, P.Y., Yang, B.K., Tong, L.L., Zhang, H.W., 2012a. Geochronological and geochemical study of the Darbut Ophiolitic Complex in the West Junggar (NW China): implications for petrogenesis and tectonic evolution. *Gondwana Res.* 21, 1037–1049.
- Yang, G.X., Li, Y.J., Santosh, M., Gu, P.Y., Yang, B.K., Zhang, B., Wang, H.B., Zhong, X., Tong, L.L., 2012b. A Neoproterozoic seamount in the Paleoasian Ocean: evidence from zircon U-Pb geochronology and geochemistry of the Mayile ophiolitic mélange in West Junggar, NW China. *Lithos* 140–141, 53–65.
- Yang, G.X., Li, Y.J., Santosh, M., Yang, B.K., Zhang, B., Tong, L.L., 2013. Geochronology and geochemistry of basalts from the Karamay ophiolitic mélange in West Junggar (NW China): implications for Devonian-Carboniferous intra-oceanic accretionary tectonics of the southern Altaids. *Geol. Soc. Am. Bull.* 125, 401–419.
- Yang, M., Wang, J.L., Wang, J.Q., Liu, C., 2015. Late Carboniferous intra-oceanic subduction and mineralization in western Junggar: evidence from the petrology, geochemistry and zircon U-Pb geochronology of I# ore-bearing granite body in Suyunhe molybdenite orefield, Xinjiang. *Acta Petrol. Sin.* 31, 523–533.
- Yin, J.Y., Yuan, C., Sun, M., Long, X.P., Zhao, G.C., Wong, K.P., Geng, H.Y., Cai, K.D., 2010. Late Carboniferous high-Mg dioritic dikes in Western Junggar, NW China: geochemical features, petrogenesis and tectonic implications. *Gondwana Res.* 17, 145–152.
- Yin, J.Y., Long, X., Yuan, C., Sun, M., Zhao, G.C., Geng, H.Y., 2013. A Late Carboniferous-Early Permian slab window in the West Junggar of NW China: geochronological and geochemical evidence from mafic to intermediate dikes. *Lithos* 175–176, 146–162.
- Yin, J.Y., Chen, W., Xiao, W.J., Yuan, C., Sun, M., Tang, G.J., Yu, S., Long, X.P., Cai, K.D., Geng, H.Y., Zhang, Y., Liu, X.Y., 2015a. Petrogenesis of Early-Permian sanukitoids from West Junggar, Northwest China: implications for Late Paleozoic crustal growth in Central Asia. *Tectonophysics* 662, 385–397.
- Yin, J.Y., Chen, W., Xiao, W.J., Yuan, C., Windley, B.F., Yu, S., Cai, K.D., 2015b. Late Silurian-early Devonian adakitic granodiorite, A-type and I-type granites in NW Junggar, NW China: partial melting of mafic lower crust and implications for slab roll-back. *Gondwana Res.* <http://dx.doi.org/10.1016/j.gr.2015.06.016>.
- Yin, J.Y., Chen, W., Yuan, C., Yu, S., Xiao, W.J., Long, X.P., Li, J., Sun, J.B., 2015c. Petrogenesis of Early Carboniferous adakitic dikes, Sawur region, northern West Junggar, NW China: implications for geodynamic evolution. *Gondwana Res.* 27, 1630–1645.

- Yuan, H.L., Gao, S., Liu, X.M., Li, H.M., Günther, D., Wu, F.Y., 2004. Accurate U-Pb Age and trace element determinations of zircon by laser ablation-inductively coupled plasma-mass spectrometry. *Geostand. Geoanal. Res.* 28, 353–370.
- Zhang, C., Huang, X., 1992. Discussions of ages and environments of ophiolite in West Junggar. *Geol. Rev.* 38, 509–524 (in Chinese with English abstract).
- Zhang, J.E., Xiao, W.J., Han, C.M., Guo, Q.Q., Mao, Q.G., Ao, S.J., 2010a. Magmatism of mid oceanic ridge subduction during Carboniferous in Western Junggar: evidence from Maliya ophiolite. *Acta Petrol. Sin.* 26, 3272–3282 (in Chinese with English abstract).
- Zhang, Q., Jin, W.J., Li, C.D., Wang, Y.L., 2010b. Revisiting the new classification of granitic rocks based on whole rock Sr and Yb contents: index. *Acta Petrol. Sin.* 26, 985–1015 (in Chinese with English abstract).
- Zhang, H., Ling, M.X., Liu, Y.L., Tu, X.L., Wang, F.Y., Li, C.Y., Liang, H.Y., Yang, X.Y., Arndt, N.T., Sun, W.D., 2013. High oxygen fugacity and slab melting linked to Cu mineralization: evidence from Dexing porphyry copper deposits, southeastern China. *J. Geol.* 121, 289–305.
- Zhang, H., Li, C.Y., Yang, X.Y., Sun, Y.L., Deng, J.H., Liang, H.Y., Wang, R.L., Wang, B.H., Wang, Y.X., Sun, W.D., 2014. Shapinggou: the largest Climax-type porphyry Mo deposit in China. *Int. Geol. Rev.* 56, 313–331.
- Zhang, X.R., Zhao, G.C., Eizenhöfer, P.R., Sun, M., Han, Y.G., Hou, W.Z., Liu, D.X., Wang, B., Liu, Q., Xu, B., 2016. Late Ordovician adakitic rocks in the Central Tianshan block, NW China: partial melting of lower continental arc crust during back-arc basin opening. *Geol. Soc. Am. Bull.* 128, 1367–1382.
- Zhao, L., He, G.Q., Zhu, Y.B., 2013. Discovery and its tectonic significance of the ophiolite in the south of Xiemisitai Mountain, West Junggar. *Geol. Bull. China* 32, 195–205 (in Chinese with English abstract).
- Zhao, P.L., Yuan, S.D., Mao, J.W., Santosh, M., Li, C.D., Hou, K.J., 2016. Geochronological and petrogeochemical constraints on the skarn deposits in Tongshanling ore district, southern Hunan Province: implications for Jurassic Cu and W metallogenic events in South China. *Ore Geol. Rev.* 78, 120–137.
- Zhong, S.H., Shen, P., Pan, H.D., Zheng, G.P., Yan, Y.H., Li, J., 2015a. Geochemistry and geochronology of ore-forming granites in Suyunhe Mo deposit, West Junggar, Xinjiang. *Miner. Deposits* 34, 39–62 (in Chinese with English abstract).
- Zhong, S.H., Shen, P., Pan, H.D., Zheng, G.P., Yan, Y.H., Li, J., 2015b. The ore-forming Fluid Study of Suyunhe Porphyry Mo Deposit, West Junggar, Xinjiang. *Acta Petrol. Sin.* 31, 449–464 (in Chinese with English abstract).